ARL TR 75-0028

AERODYNAMIC CALIBRATION OF THE AEROSPACE RESEARCH LABORATORIES M = 6 HIGH REYNOLDS NUMBER FACILITY

ANTHONY W. FIORE
C. HERBERT LAW
THEORETICAL AERODYNAMICS RESEARCH LABORATORY/ARL

FEBRUARY 1975

FINAL REPORT DECEMBER 1973 – MARCH 1974

AEROSPACE RESEARCH LABORATORIES/LH
Building 450 – Area B
Wright-Patterson Air Force Base, Ohio 45433

AIR FORCE SYSTEMS COMMAND
United States Air Force

NOTICES

When Government drawings, specifications, or other data are used for any purpose other than in connection with a definitely related Government procurement operation, the United States Government thereby incurs no responsibility nor any obligation whatsoever; and the fact that the Government may have formulated, furnished, or in any way supplied the said drawings, specifications, or other data, is not to be regarded by implication or otherwise as in any manner licensing the holder or any other person or corporation, or conveying any rights or permission to manufacture, use, or sell any patented invention that may in any way be related thereto.

Organizations or individuals receiving reports via Aerospace Research Laboratories automatic mailing lists should refer to the ARL number of the report received when corresponding about change of address or cancellation. Such changes should be directed to the specific laboratory orginating the report. Do not return this copy; retain or destroy.

Reports are not stocked by the Aerospace Research Laboratories. Copies may be obtained from:

National Technical Information Services
Clearinghouse
Springfield, VA 22151

This technical report has been reviewed and is approved for publication.

FOR THE COMMANDER:

Elizabeth Day

ELIZABETH DAY
Technical Documents
and STINFO Office

This report has been reviewed and cleared for open publication and public release by the appropriate Office of Information in accordance with AFR 190-12 and DODD 5230.0. There is no objection to unlimited distribution of this report to the public at large, or by DDC to the National Technical Information Service.

AIR FORCE/56780/7 July 1975 — 100

SECURITY CLASSIFICATION OF THIS PAGE (When Data Entered)

REPORT DOCUMENTATION PAGE

READ INSTRUCTIONS BEFORE COMPLETING FORM

1. REPORT NUMBER: ARL [redacted]75-0028	2. GOVT ACCESSION NO.
3. RECIPIENT'S CATALOG NUMBER	
4. TITLE (and Subtitle): Aerodynamic Calibration of The Aerospace Research Laboratories' M=6 High Reynolds Number Facility	5. TYPE OF REPORT & PERIOD COVERED: [redacted] Final rep't. Dec[redacted]73 - Mar[redacted]74
	6. PERFORMING ORG. REPORT NUMBER
7. AUTHOR(s): Anthony W. Fiore [redacted] C. Herbert Law	8. CONTRACT OR GRANT NUMBER(s)
9. PERFORMING ORGANIZATION NAME AND ADDRESS: Aerospace Research Laboratories (AFSC) Theoretical Aerodynamics Research Laboratory/ARL Wright-Patterson AFB, Ohio 45433	10. PROGRAM ELEMENT, PROJECT, TASK AREA & WORK UNIT NUMBERS: [redacted] 7064[redacted]
11. CONTROLLING OFFICE NAME AND ADDRESS: Aerospace Research Laboratories (LH) Bldg 450, Area B Wright-Patterson AFB, Ohio 45433	12. REPORT DATE: Feb[redacted]75
	13. NUMBER OF PAGES: 62
14. MONITORING AGENCY NAME & ADDRESS (if different from Controlling Office)	15. SECURITY CLASS. (of this report): Unclassified
	15a. DECLASSIFICATION DOWNGRADING SCHEDULE

16. DISTRIBUTION STATEMENT (of this Report)

Approved for public release; distribution unlimited.

17. DISTRIBUTION STATEMENT (of the abstract entered in Block 20, if different from Report)

18. SUPPLEMENTARY NOTES

19. KEY WORDS (Continue on reverse side if necessary and identify by block number)

Wind Tunnels
High Reynolds number facility
Aerodynamic Calibration
hypersonics

20. ABSTRACT (Continue on reverse side if necessary and identify by block number)

This report describes the Aerospace Research Laboratories' Mach 6 high Reynolds number wind tunnel and its aerodynamic calibration. This facility operates at a Mach number of approximately 6 over a unit Reynolds number range of 10 sup 7 to 3 x 10 sup 7 per foot. The Unit Reynolds number is varied by changing the stagnation pressure from 700 through 2100 psia while the stagnation temperature is held constant at 100 deg. R. The aerodynamic calibration consisted of the determination of the actual free stream Mach number distribution, the free stream total temperature distribution, the flow angularity within the test core, and

DD FORM 1 JAN 73 1473 EDITION OF 1 NOV 65 IS OBSOLETE

Unclassified

SECURITY CLASSIFICATION OF THIS PAGE (When Data Entered)

some insight into tunnel blockage conditions. The Mach number and total temperature distribution tests were conducted simultaneously and were carried out at three stagnation pressures of 700, 1400, and 2100 psia corresponding to unit Reynolds numbers of 9.76 x 10 sup 6, 18.77 x 10 sup 6, and 30.27 x 10 sup 6 per foot. The flow angularity and blockage tests were conducted at one stagnation pressure, i.e., 700 psia corresponding to a unit Reynolds number of 9.76 x 10 sup 6 per foot. The results indicate the free stream Mach number has a root-mean-square value of 5.88 and is independent of the unit Reynolds number. The Mach number gradients in both the lateral and longitudinal direction were negligibly small. The total temperature distribution within the test core was invariant with unit Reynolds number and within plus 2% of the stagnation temperature. The test core was approximately 10 inches in diameter as compared to a nozzle outlet diameter of 12.346 inches. Flow angularity within the test core remained relatively small and never exceeded plus and minus 0.05 degrees.

PREFACE

This report was prepared by Dr. Anthony W. Fiore and Dr. C. Herbert Law of the Theoretical Aerodynamics Research Laboratory, Aerospace Research Laboratories, Air Force Systems Command, United States Air Force. The investigation was conducted under Project 7064 entitled, "High Velocity Fluid Mechanics."

TABLE OF CONTENTS

LIST OF ILLUSTRATIONS

LIST OF TABLES

SECTION I

INTRODUCTION

The need for aerodynamic test data at high Reynolds numbers has become increasingly apparent as the result of identifying critical problem areas associated with new and advanced Air Force weapons systems. Fundamental information in the supersonic and hypersonic high Reynolds number flow regime was scant with little experimental data pertaining to pure turbulent boundary layers, flow field interactions, heat transfer rates, and skin friction measurements under turbulent flow conditions.

With the need established, two facilities were designed and built at Wright-Patterson Air Force Base to simulate supersonic and hypersonic high Reynolds number flight. One was a Mach number 3 wind tunnel while the second was a Mach number 6 facility operating in the unit Reynolds number range from 10^7 to 3×10^7 per foot. The Mach 3 wind tunnel design and calibration have already been reported in reference 1; this report describes the Mach 6 wind tunnel and its aerodynamic calibration. The preliminary design for this facility was carried out by The Theoretical Aerodynamics Laboratory while the mechanical design and check out were conducted by The Fluid Mechanics Research Laboratory. The aerodynamic calibration, which is reported here, was done by The Theoretical Aerodynamics Laboratory between December 1973 and March 1974.

SECTION II

DESCRIPTION OF FACILITY

The Mach 6 facility was designed to produce a maximum free stream unit Reynolds number of approximately 3×10^7 per foot at a stagnation pressure of 2100 psia and a stagnation temperature of 1100°R. The test core is produced by a contoured axisymmetric nozzle with an exit diameter of 12.346 inches. The nozzle contour was designed with boundary layer correction[2] to give a nominal uniform exit Mach number of 6. The tunnel configuration is shown in Fig. 1 and the nozzle coordinates are presented in Table I. The facility operates over a stagnation pressure range from 700 to 2100 psia with a fixed stagnation temperature of approximately 1100°R. The supply air is heated by a pebble bed storage heater which allows run times up to 300 seconds at the maximum mass flow rate of 90 pounds per second at a stagnation pressure of 2100 psia.

The open jet test region is variable in length from 17.5 to 27.5 inches in 5-inch increments. Diffuser collection is achieved through a conical collector with a capture diameter of 18 inches. The air is exhausted to the atmosphere through a fixed geometry diffuser and silencer.

The air storage system for this facility consists of approximately 12,000 cubic feet of air at 3000 psig. Three air compressors are used to compress atmospheric air to 3000 psia. Each compressor makes use of four stages of compression. At the end of each stage of compression both water and oil vapor are removed. Prior to entering the storage system, the compressed air is dried through a series of silica gel dryers to a dew point of -100° F.

The air supply is isolated from the test facility by two electrically operated main air valves. Further isolation from the M=6 wind tunnel is maintained by a hydraulically operated isolation valve. A block diagram of these components is presented in Fig. 2.

The pebble bed heater vessel, which contains 50,000 pounds of 3/4-inch diameter stainless steel balls, is used to heat the test medium to an operating temperature of 1100^{0}R. Two electrical resistance heaters with a capacity of 700 cfm of air at a working pressure of 30 psig are used to preheat the air which is circulated through the vessel for approximately 12 hours prior to initiating wind tunnel tests. Power input to each heater is 90 kilowatts maximum. The regeneration cycle is fully automatic and controlled by a circuit breaker and thermocouple feedback controller to maintain the heater at the operating temperature. Regeneration of the heater vessel between runs requires no more than four hours of heating.

The sequence of operation, as outlined in Fig. 2, proceeds as follows: The main air valves and the isolation valve are opened to provide the supply air at approximately 3000 psig and ambient temperature. Storage heater vessel pressurization is then accomplished under automatic control through the control valve. When the pressure in the heater vessel reaches the selected stagnation pressure, the heater shut-off valve opens automatically, and flow is established through the wind tunnel. The proper stagnation pressure is maintained automatically by a controller which opens the control valve in relation to the stagnation pressure transducer feedback circuit. The air exits the wind tunnel through an exhaust valve and silencer to the atmosphere.

A sealed test cabin encloses the nozzle exit, test region, diffuser collector, and model support system. Instrumentation access parts and viewing windows are available for data acquisition. Prior to the initiation of a test, the model is retracted into the bottom of the test cabin. After establishment of steady free stream conditions, the model is injected into the test region by remote control, and appropriate data are recorded. Prior to termination of the test, the model is retracted into the bottom of the test cabin. Injection and retraction time is approximately two seconds.

Two model support systems are available; the first system is a pitch-pause system used to pitch a model about a fixed point of rotation on the tunnel centerline. The second is a rigid nonpitching platform which allows for off-centerline mounting and remotely controlled axial translation. The pitch-pause model support system provides an angle of attack variation from -25^{o} to $+25^{o}$ with a resolution of 0.05^{o}. In the manual mode of operation, any pitch angle can be set and changed at will during a test. Automatic angular rotation from -25^{o} to $+25^{o}$ can be achieved in one second. In the automatic mode, the pitching increment and direction are preselected. When the automatic control is initiated, the model pitches from zero to the next angle of attack with an interval of pause equivalent to the preselected increment and then pitches to the next angle of attack. The cycle continues until a preselected limit is reached or manual termination is initiated. When the angle of attack limit is reached, the model automatically returns to zero pitch, and the model retracts out of the flow. An override is provided so the cycle may be manually interrupted at any time. Injection and retraction of the model and its support system can be performed only while the model is at zero degrees angle of attack.

The platform model support system permits the models to be mounted at any horizontal or vertical position at some fixed angle of attack within the test region. The axial position of tnis system may be varied, from the nozzle exit to the diffuser collector inlet. Translation constraints depend only on model configuration and size. Resolution of the axial position is 0.001 inch, and the maximum translation speed is 0.1 inch per second. This particular system may be injected or retracted, provided the model will clear both the nozzle outlet and diffuser inlet.

SECTION III

DESCRIPTION OF THE DATA ACQUISITION SYSTEM

The Mach 6 wind tunnel calibration required making measurements of pressure, temperature, model angle of attack, and flow field schlieren photographs. All pressures were measured with variable reluctance transducers. Temperatures were measured with iron/constantan thermocouples referred to a temperature of 150^{0} F. Separate amplifiers within the reference block were used to amplify the thermocouple output from 0 to 10 volts. A regulated power supply and precision potentiometer were used to measure the model axial position and angle of attack.

The data recording instrumentation system consisted of precision digital volt meters, XY plotters, and a 36-channel visicorder. Daily calibrations of all components gave reliable accuracies of one half percent full scale.

Schlieren photographs were obtained by using a standard single pass system and a continuous light source.

In addition to model measurements, certain basic wind tunnel parameters were measured. These included the stagnation pressure and temperature, test cabin pressure and temperature, and both nozzle and diffuser wall static pressure distributors. Multiple pressure measurements were made by a single pressure transducer through a scanivalve.

By acquiring data in analog form, time dependent variables could be monitored to obtain correct steady state values. Scanivalve measurements could be made at a rate of one pressure per second. Individual

signals, such as stagnation pressure and temperature, and model measurements were monitored to insure that proper stabilization of the flow field was attained prior to data recording. During a typical 60-second run, variations in stagnation conditions were undetectable when compared with the preset stagnation values of pressure and temperature. Total stabilization time was found to be approximately five seconds.

SECTION IV

DESCRIPTION OF CALIBRATION MODELS

The calibration models are presented in Figs. 3 and 4. These models were designed to obtain the flow angularity and both lateral and longitudinal Mach number distributions, and the total enthalpy distribution at several points within the test region. In addition, a few blockage tests were made by using the configurations shown in Fig. 5, whose corresponding notation is given in Tables II and III.

The Mach number and total enthalpy rake consisted of nine total pressure probes and eight modified Winkler total temperature probes. The alternating total pressure and temperature probes were spaced on the rake at 1-inch intervals. The complete rake assembly could be moved laterally across the test region to give both total pressure and temperature measurements at 1/4 inch intervals across a span of 18 inches. With the rake mounted on the platform support system both lateral Mach number and total enthalpy distributions could be obtained at any axial station between the nozzle exit and within five inches of the collector inlet. The Mach number and total enthalpy rake is shown in Fig. 4.

The angularity cone, which is shown in Fig 3, consisted of a 15^{o} half angle cone with two surface pressure orifices placed on the upper and lower surfaces, respectively, and at the same distance from the model tip corresponding to the point of rotation of the model. An electric motor and precision potentiometer were mounted in the support strut for actuating and measuring the cone angle of attack, which could be varied a maximum of $\pm 2.0^{o}$ with a resolution of approximately 0.01^{o}. By pitching the cone and monitoring the pressure

difference between the two pressure orifices with a variable reluctance transducer, the local flow angularity could be determined as that angle which gave zero pressure difference between the two pressure orifices. Axial and lateral positioning of the angularity cone was achieved by manual movement of the cone model on the platform support system.

Three basic blockage model configurations were investigated, a 10^{o} half angle cone, a 15^{o} half angle cone, and a 10^{o} half angle wedge. The blockage model configurations are shown in Fig. 5, and the notation is defined in Tables II and III. For each model three variables were investigated, model nose radius, base diameter or height, and angle of attack. Without changing the basic body shape, the nose radius and/or base diameter (base height for the wedge) could be changed independently. In each case the angle of attack could be varied from -25^{o} to $+25^{o}$ about a center of rotation approximately nine inches downstream of the nozzle exit.

SECTION V

DESCRIPTION OF AERODYNAMIC CALIBRATION

The aerodynamic calibration of the M=6 high Reynolds number facility consisted of the following tests:

1) Measurements to determine the actual free stream Mach number distribution and the lateral and longitudinal Mach number gradients.

2) Measurements to determine the free stream total temperature distribution.

3) Measurements to determine the magnitude of the flow angularity in the free stream.

4) Blockage tests to determine model configuration and size limitations.

Tests were conducted at a nominal stagnation temperature of 1100^{o} R and three values of stagnation pressure, namely, 700, 1400, and 2100 psia, which correspond to unit Reynolds numbers of 9.76×10^{6}, 18.77×10^{6}, and 30.27×10^{6} per foot. The flow angularity and tunnel blockage tests were conducted at one stagnation pressure of 700 psia. corresponding to a unit Reynolds Number of 9.76×10^{6} per foot.

1. LATERAL AND LONGITUDINAL MACH NUMBER DISTRIBUTIONS

The Mach number distributions were obtained by using the total pressure rake shown in Fig. 4. Tests were conducted at three longitudinal stations, 2.5, 5.75, and 9.00 inches from the nozzle exit plane. Measurements of total pressure were made across the free stream every 0.5 inch.

The local Mach number was obtained by computer iteration of Rayleigh's pitot equation. The results are presented in Figs. 6 through 8. In Fig. 6, for x=2.5 inches and a unit Reynolds Number of 9.76×10^6 per foot the local Mach number varies almost linearly from the tunnel centerline, where the Mach number is 5.82, to the outer edge of the jet at $y=\pm 5$ inches, where the Mach number is 5.95. In this case, the root-mean-square (r.m.s.) value of all the points is 5.87. As the unit Reynolds number is increased, it should be noted that:

1) The r.m.s. Mach number varies only slightly with increasing unit Reynolds number. It was 5.90 at a unit Reynolds number of 18.77×10^6 per foot and 5.86 at 30.27×10^6 per foot.

2) The lateral Mach number distribution is almost invariant with increasing unit Reynolds number. The maximum variation occurs near the tunnel centerline and is due to Mach wave focusing effect, which is typical of an axisymmetric nozzle. This effect changes with longitudinal distance, as is observed in Fig. 7 for x= 5.75 inches and Fig. 8, where x= 9.00 inches. At all axial stations and unit Reynolds Numbers, the local Mach numbers are within $\pm$ 1.5% of the calculated r.m.s. value of the free stream Mach number of 5.88.

The unit Reynolds Number effect on the lateral Mach Number distribution is shown in Fig. 9. The data are presented as a plot of local Mach Number versus lateral distance with the average unit Reynolds number as a parameter. These data show that the lateral Mach Number distributions are independent of the unit Reynolds Number throughout the test regime.

The variation of the r.m.s. free stream Mach Number with longitudinal distance is shown in Fig. 10. These data indicate that the r.m.s. Mach Number increases very slightly with increasing distance from the nozzle exit, and it varies from 5.88 at 2.5 inches from nozzle exit to 5.90 at a distance of 9 inches from the exit plane.

The longitudinal pressure gradients were calculated by differentation of the energy equation. The results of these calculations are presented in Fig. 11, where both the Mach Number and static pressure gradients are shown to be invariant with longitudinal distance; however, there is a very slight variation with unit Reynolds Number which is considered to be well within the experimental accuracy of these tests. The Mach Number gradient was found to vary from 0.0026 to 0.0054 of a Mach Number per inch. The corresponding longitudinal static pressure gradient varied from -0.0015 to -0.0087 psia/inch over the same range of unit Reynolds Numbers. The average overall values of these gradients were taken as $dM/dx = 0.004$ in.$^{-1}$ and $dp/dx = 0.0051$ psia/inch.

2. LATERAL AND LONGITUDINAL TOTAL TEMPERATURE DISTRIBUTIONS

The nondimensional lateral total temperature distributions are presented in Figs. 12, 13, and 14 for axial distances of 2.5, 5.75, and 9.00 inches, respectively. At each longitudinal station total temperature measurements were obtained for three unit Reynolds numbers. Measurements were made by using a series of modified Winkler total temperature probes mounted on the rake shown in Fig. 4. In general, the results show

that the total temperature distributions in the free stream were within $\pm$ 2% of the tunnel stagnation temperature, which is within the experimental accuracy of the measurements. In addition, the free stream total temperature distributions were invariant with unit Reynolds number.

3. TEST CORE SIZE

A plot of local Mach number versus lateral distance at 2.5 inches from the nozzle exit is presented in Fig. 15 for three free stream unit Reynolds numbers. The test core was found to be approximately 10 inches in diameter as compared to the nozzle exit diameter of 12.346 inches, and was essentially independent of the unit Reynolds number. It also shows that the free shear layer extends in an axisymmetric manner around the test core from y = $\pm$5 to y = $\pm$6.17 inches.

4. NOZZLE WALL STATIC PRESSURE AND MACH NUMBER MEASUREMENTS

Measurements of static pressure along the nozzle wall are presented in Fig. 16 and are compared with inviscid theory. These data are for three different unit Reynolds numbers. The measured wall pressures compare well with the inviscid theory up to a distance of 11.5 inches from the throat. Beyond this point the measured pressures are slightly higher than the inviscid values. In order to check this trend the local static pressure in the free jet at each unit Reynolds number was calculated from Reynold's pitot equation by making use of the r.m.s. Mach number and the tunnel stagnation pressure. These points are shown as "open" data points in Fig. 16, and they seem to confirm the previously mentioned trend.

The corresponding local Mach number distribution down the nozzle is presented in Fig. 17, where this effect can be seen more clearly. The calculated Mach numbers agree with the inviscid theory up to X_t = 11.5 inches, where the Mach number is approximately 3.92; then, as the distance from the throat is increased to the nozzle exit plane, the calculated Mach number is less than the inviscid value. The difference between the data and theory may be attributed to both boundary layer displacement effects and the fact that at hypersonic speeds ($M \geq 5$), the pressure gradient through the boundary layer is no longer zero [3].

5. FREE STREAM FLOW ANGULARITY

The flow angularity measurements were made with the sharp cone model shown in Fig. 3. Measurements were made at a stagnation pressure of 719 psia and a stagnation temperature near 1095 ^{o}R corresponding to a free stream unit Reynolds number of 9.76×10^6 per foot. Tests were conducted at the three longitudinal stations of 2.5, 5.75, and 9.00 inches from the nozzle exit plane and at three lateral stations of y= 0 and $\pm$ 3.67 inches. The local flow angularity at each station was obtained by averaging the measurements made with the model in the upright ($\phi = 0^{o}$) and inverted ($\phi = 180^{o}$) positions. The purpose for testing in both positions was to take into account small irregularities in the fabrication process of the model and its orifices. A typical set of results is presented in Fig. 18, where Δp is plotted versus angle of attack for $\phi = 0^{o}$ and $\phi = 180^{o}$. The flow angularity is taken as the average (and with opposite sign) of the two angles corresponding to the case where $\Delta p = 0$, which is $\alpha_a = +0.07^{o}$. All the flow angularity

measurements were made by this technique; the results are shown in Figs. 19 and 20.

The variation of flow angularity with lateral distance is summarized in Fig. 19. At a distance of 2.5 inches from the nozzle exit plane the angularity varies linearly from 0.025^{o} at y = 3.67" to 0.05^{o} at y = +3.67". At X = 5.75" the angularity increases from -0.05^{o} on the west side to $+0.05^{o}$ at the tunnel centerline and remains constant at $+0.05^{o}$ in the range $0 \leq y \leq +3.67$". As the distance from the nozzle exit plane is increased to 9.00 inches a similiar trend exists; i.e., on the west side $\alpha_a = +0.02^{o}$ while at the tunnel centerline it is $+0.04^{o}$, and on the east side of the nozzle it is $+0.045^{o}$.

Assuming linear variation in the flow angularity with lateral distance, the gradients are 0.0034 degree/inch at 2.5 and 5.75 inches from nozzle outlet and 0.00164 degree/inch at 9.00 inches from the nozzle exit plane.

The longitudinal variation in flow angularity was obtained by cross-plotting the data shown in Fig. 19 and is presented in Fig. 20. The angularity is constant with increasing axial distance on both the east side of the nozzle and on the centerline; its value is +0.045. On the centerline, its value is +0.045. On the west side of the nozzle the flow angularity is nearly nonexistent. This variation across the jet is not fully understood. In any case, it is concluded that the flow angularity and its gradients in both directions are insignificantly small. The angularity never exceeds $\pm 0.05^{o}$, and the gradients are of the order of 0.0025 degree/inch.

6. BLOCKAGE TESTS

Two model configurations which directly influence tunnel blockage limitations were investigated. For a particular model configuration, the total frontal area cannot exceed certain limits without destroying the diffuser performance. Also, the model nose radius of curvature creates a bow shock which interacts with the tunnel free shear layer to limit the nozzle performance. Another parameter which influences both of these effects is the model angle of attack. As the angle of attack increases, the effective model cross-sectional area and the influence of the bow shock on the free shear layer increase.

The three basic configurations shown in Fig. 5 were investigated, a 10^{0} cone, a 15^{0} cone, and a 10^{0} wedge. All tests were performed at the lowest unit Reynolds number of 9.76×10^{6} per foot.

Figures 21 and 22 present the blockage data for the basic model shape of a 15^{0} cone. Here the cabin pressure is plotted as a function of the model angle of attack. The cabin pressure level is used as an indicator of the nozzle's ability to achieve hypersonic flow in the test core. Figure 21 shows the effects of a variable base diameter. As the base diameter or frontal area is increased, the maximum allowable angle of attack is reduced. The symmetry about zero angle of attack indicates that the model support strut does not significantly contribute to the blockage constraints. Figure 22 shows the effect of nose shape for the smallest base diameter model; although no detrimental effects of nose bluntness (stronger bow shock) are evident here, these effects may become more apparent for larger base diameters.

Figures 23 through 27 show the results for the 10^{o} wedge model. The effects of the base area are shown in Fig. 23 for the sharp nose and Fig. 24 for the round nose wedge. As in the case of the 15^{o} cone it is noted that as the base area increases the maximum allowable angle of attack decreases; however, some nonsymmetry effects are now evident. For example in Fig. 23 where H = 2.00 inches larger negative angles of attack can be achieved as compared to the positive angles of attack for the same model configuration.

Figures 25, 26, and 27 present the effects of nose shape for the 10^{o} wedge model. Except for the symmetry effects already discussed, the nose shape has little effect on blockage limitations, with two exceptions. In Fig. 25, the round nose configuration reduces the maximum allowable negative angle of attack, and, in Fig. 27, the square nose configurations failed to remain in flow at any angle of attack. It is possible that a large base area and a strong bow shock combined to collapse the tunnel jet. The tunnel might have started if this particular nose shape were equipped with a smaller base area.

Figure 28 shows a comparison between a 15^{o} and a 10^{o} cone with round noses of different radii but the same base area. The effects of different body shapes or nose radii are not apparent.

It should be pointed out that, although the cabin pressure was monitored to indicate in and out of flow conditions, the schlieren system was also monitored to record the flow field characteristics. As the cabin pressure increases, an axially symmetric shock wave is generated at the nozzle exit

because of the over-expanded nature of the free jet cased by increasing cabin pressure. As shown in Figure 29, this shock wave may interfere with the compressure surface of the model, thereby producing undesirable effects. The wind tunnel may remain in flow even through this undesirable interaction exists. Particular configurations or circumstances will require monitoring such items as the model compression side pressure distribution, the model wake, and flow field visualization through schlieren pictures to insure the data are valid.

SECTION VI

CONCLUSIONS

In summary, this report contains a description of the Aerospace Research Laboratories' M=6 high Reynolds number wind tunnel and its aerodynamic characteristics. The facility operates at a stagnation temperature near 1100°R and a stagnation pressure of $700 \leq P_o$ (psia) ≤ 2100 at a nominal Mach number of six, corresponding to a unit Reynolds number range of $9.76 \times 10^6 \leq \frac{R_e}{\ell}$ (ft^{-1}) $\leq 30.27 \times 10^6$. The facility's maximum running time is approximately 100 seconds for a maximum mass flow rate of 90 lbs/sec at the highest unit Reynolds number of 30.27×10^6 per foot.

Listed below are the results of the aerodynamic calibration of this facility:

1) The free stream Mach number was found to be essentially independent of unit Reynolds numbers with an overall root-mean-square value of 5.88.

2) The local Mach number and static pressure gradients were insignificantly small and within the experimental accuracy of the measurements.

3) The size of the test core was approximately 10 inches in diameter as compared to a nozzle outlet diameter of 12,347 inches.

4) The lateral and longitudinal total temperature distribution in the test core was invariant with unit Reynolds number and within +2% of the tunnel stagnation temperature.

5) The flow field angularity in the test core was negligible and never exceeded values of $\pm$ 0.05 degree.

6) Some blockage tests were conducted with both cones and wedges with various nose radii and base sizes. Precautions must be taken to avoid excessively large frontal area blockage and interference of the nozzle shock on the model compression surface flow field.

TABLE I

M = 6 NOZZLE COORDINATES AND LOCAL INVISCID MACH NUMBER

X_t	r	M	X_t	r	M	X_t	r	M
INCH	INCH	—	INCH	INCH	—	INCH	INCH	—
1.646	.8215	1.0000	26.246	4.6277	5.303	50.846	5.9960	6.003
2.246	.9279	1.631	26.846	4.6864	5.336	51.446	6.0094	6.009
2.846	1.0343	1.924	27.446	4.7434	5.368	52.046	6.0220	6.015
3.446	1.1409	2.156	28.046	4.7989	5.398	52.646	6.0340	6.020
4.046	1.2475	2.355	28.646	4.8528	5.427	53.246	6.0454	6.026
4.646	1.3342	2.500	29.246	4.9051	5.456	53.846	6.0561	6.031
5.246	1.4609	2.693	29.846	4.9560	5.483	54.446	6.0662	6.035
5.846	1.5677	2.842	30.446	5.0054	5.509	55.046	6.0757	6.040
6.446	1.6746	2.980	31.046	5.0534	5.535	55.646	6.0846	6.044
7.046	1.7816	3.110	31.646	5.0999	5.559	56.246	6.0930	6.048
7.646	1.8886	3.233	32.246	5.1451	5.583	56.846	6.1007	6.051
8.246	1.9957	3.350	32.846	5.1890	5.605	57.446	6.1081	6.055
8.846	2.1029	3.462	33.446	5.2315	5.627	58.046	6.1149	6.058
9.446	2.2101	3.569	34.046	5.2728	5.648	58.646	6.1211	6.061
10.046	2.3173	3.671	34.646	5.3128	5.669	59.246	6.1268	6.063
10.646	2.4247	3.770	35.246	5.3515	5.689	59.846	6.1321	6.066
11.246	2.5320	3.866	35.846	5.3890	5.708	60.446	6.1369	6.068
11.846	2.6394	3.958	36.446	5.4253	5.726	61.046	6.1413	6.070
12.446	2.7459	4.047	37.046	5.4604	5.743	61.646	6.1453	6.072
13.046	2.8509	4.131	37.646	5.4945	5.760	62.246	6.1788	6.087
13.646	2.9539	4.212	38.246	5.5273	5.777	62.846	6.1521	6.075
14.246	3.0550	4.290	38.846	5.5591	5.792	63.446	6.1550	6.076
14.846	3.1540	4.363	39.446	5.5899	5.808	64.046	6.1576	6.078
15.446	3.2506	4.434	40.046	5.6195	5.822	64.646	6.1599	6.079
16.046	3.3449	4.501	40.646	5.6482	5.836	65.246	6.1620	6.080
16.646	3.4370	4.566	41.246	5.6758	5.850	65.846	6.1638	6.080
17.246	3.5268	4.627	41.846	5.7025	5.863	66.446	6.1654	6.081
17.846	3.6144	4.686	42.446	5.7281	5.875	67.046	6.1668	6.082
18.446	3.6999	4.743	43.046	5.7529	5.887	67.646	6.1681	6.082
19.046	3.7832	4.797	43.646	5.7766	5.898	68.246	6.1694	6.083
19.646	3.8643	4.849	44.246	5.7995	5.909	68.846	6.1706	6.084
20.246	3.9433	4.899	44.846	5.8215	5.920	69.446	6.1717	6.084
20.846	4.0203	4.947	45.446	5.8426	5.928	70.046	6.1728	6.085
21.446	4.0953	4.993	46.046	5.8628	5.940	70.156	6.1730	6.085
22.046	4.1684	5.037	46.646	5.8822	5.949			
22.646	4.2394	5.079	47.246	5.9008	5.958			
23.246	4.3086	5.120	47.846	5.9186	5.966			
23.846	4.3760	5.160	48.446	5.9356	5.974			
24.446	4.4416	5.198	49.046	5.9518	5.982			
25.046	4.5054	5.234	49.646	5.9673	5.989			
25.646	4.5674	5.270	50.246	5.982	5.996			

TABLE II

BLOCKAGE MODEL DIMENSIONS

MODELS	M1 : M2 : M3 :	10 DEG. HALF ANGLE CONE 15 DEG. HALF ANGLE CONE 10 DEG. HALF ANGLE WEDGE, SPAN = 7.75 IN.
NOSES	N1 : N2,1 : N2,2 : N2,3 : N3,1 : N3,2 : N3,3 :	ROUND, 1.0 IN. RADIUS SHARP, 0 IN. RADIUS ROUND, 3/8 IN. RADIUS SQUARE, INFINITY RADIUS SHARP, 0 IN. RADIUS ROUND, 3/8 IN. RADIUS SQUARE, INFINITY RADIUS
BASES	B1 : B2,1 : B2,2 : B2,3 : B3,1 : B3,2 : B3,3 :	4.5 IN. DIAM. 4.5 IN. DIAM. 5.0 IN. DIAM. 5.375 IN. DIAM. 1.5 IN. HEIGHT 1.75 IN. HEIGHT 2.0 IN. HEIGHT

TABLE III

BLOCKAGE MODEL CONFIGURATIONS TESTED

CONFIG-URATION	MODEL	NOSE	BASE	BLOCK. AREA/ NOZ. EX. AREA AT $\alpha = 0°$
1	M1	N1	B1	0.141
2	M2	N2,1	B2,1	0.141
3	M2	N2,1	B2,2	0.174
4	M2	N2,1	B2,3	0.201
5	M2	N2,2	B2,1	0.141
6	M2	N2,3	B2,1	0.141
7	M3	N3,1	B3,1	0.103
8	M3	N3,1	B3,2	0.120
9	M3	N3,1	B3,3	0.137
10	M3	N3,2	B3,1	0.103
11	M3	N3,2	B3,2	0.120
12	M3	N3,2	B3,3	0.137
13	M3	N3,3	B3,3	0.137

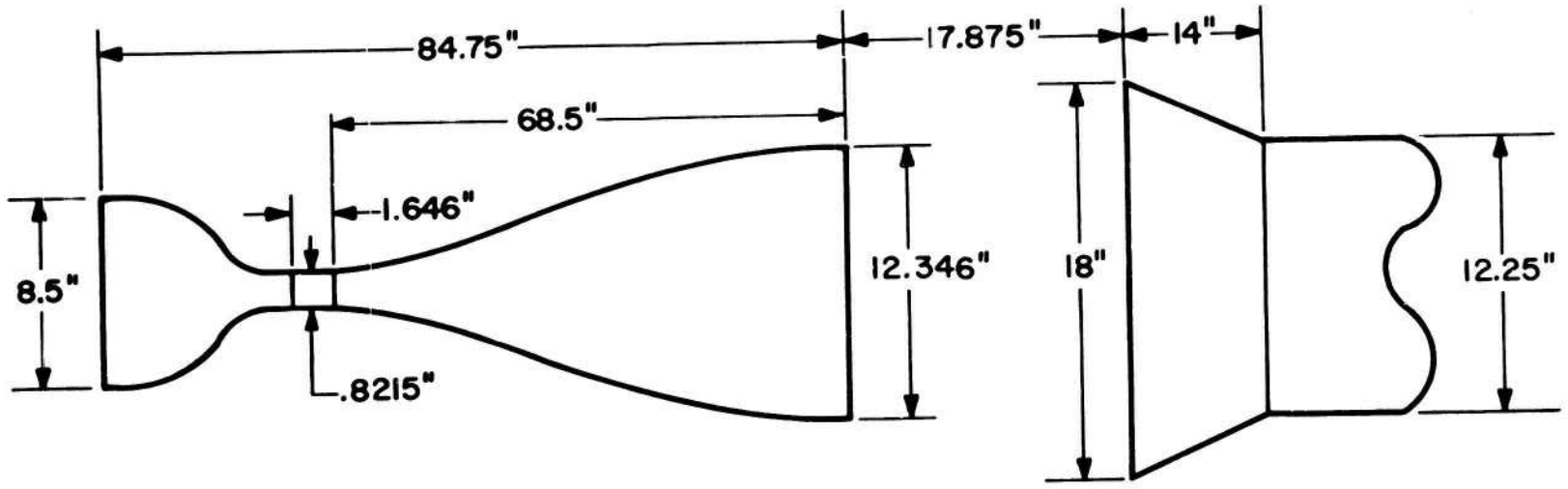

Figure 1. M=6 Wind Tunnel Nozzle, Jet, and Collector Configuration

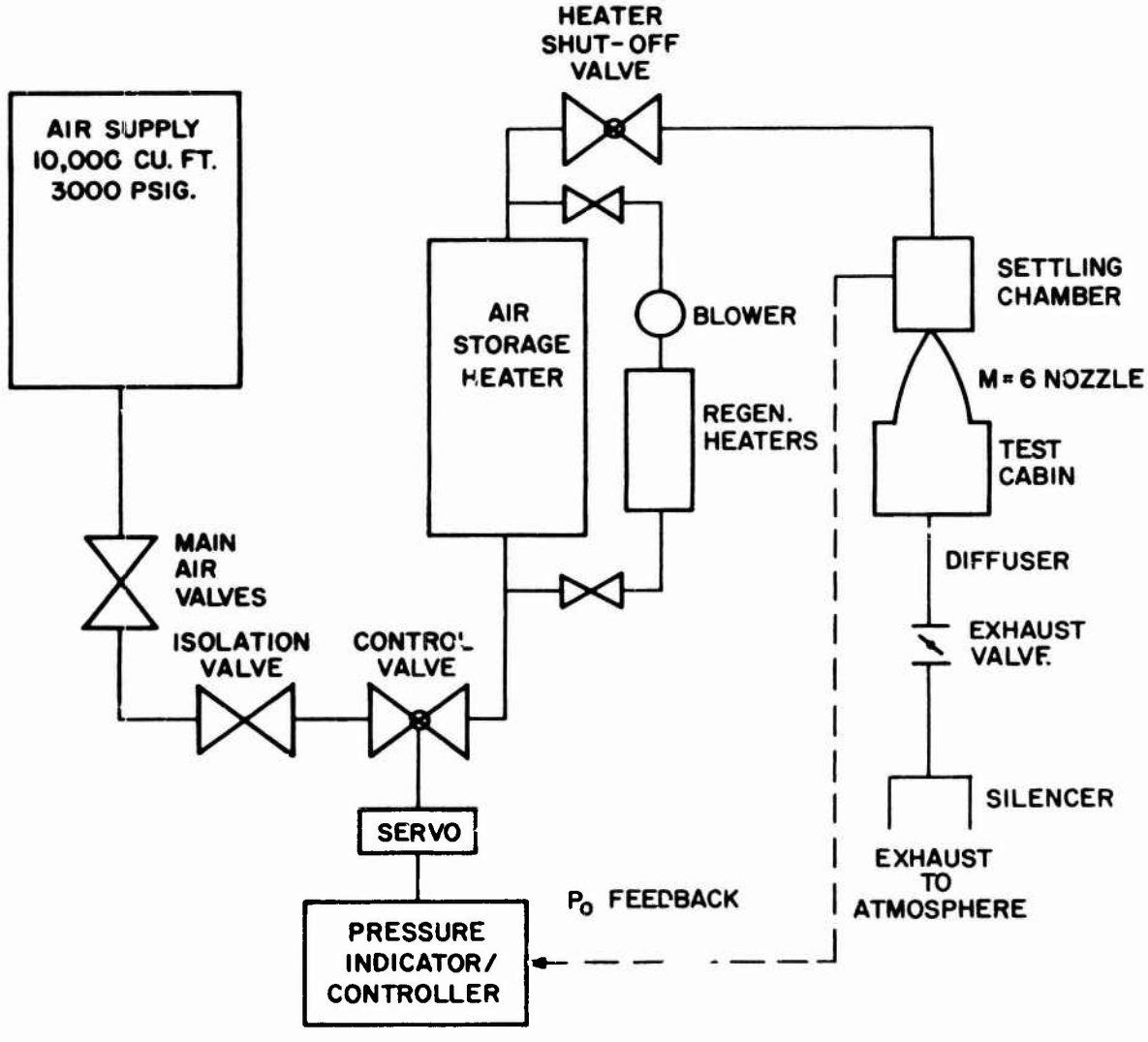

Figure 2. M=6 Wind Tunnel Operation Process Diagram

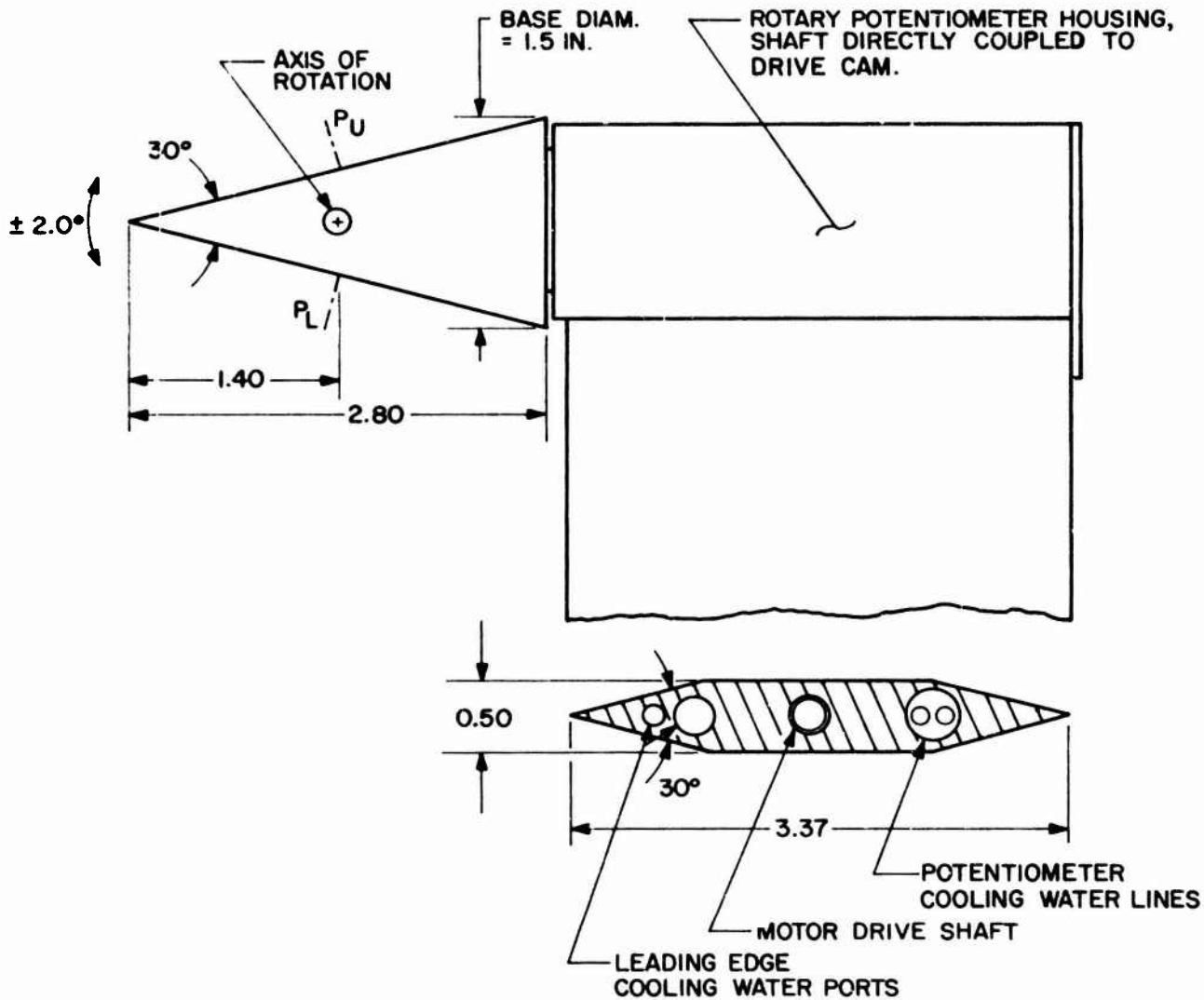

Figure 3. Angularity Cone Configuration

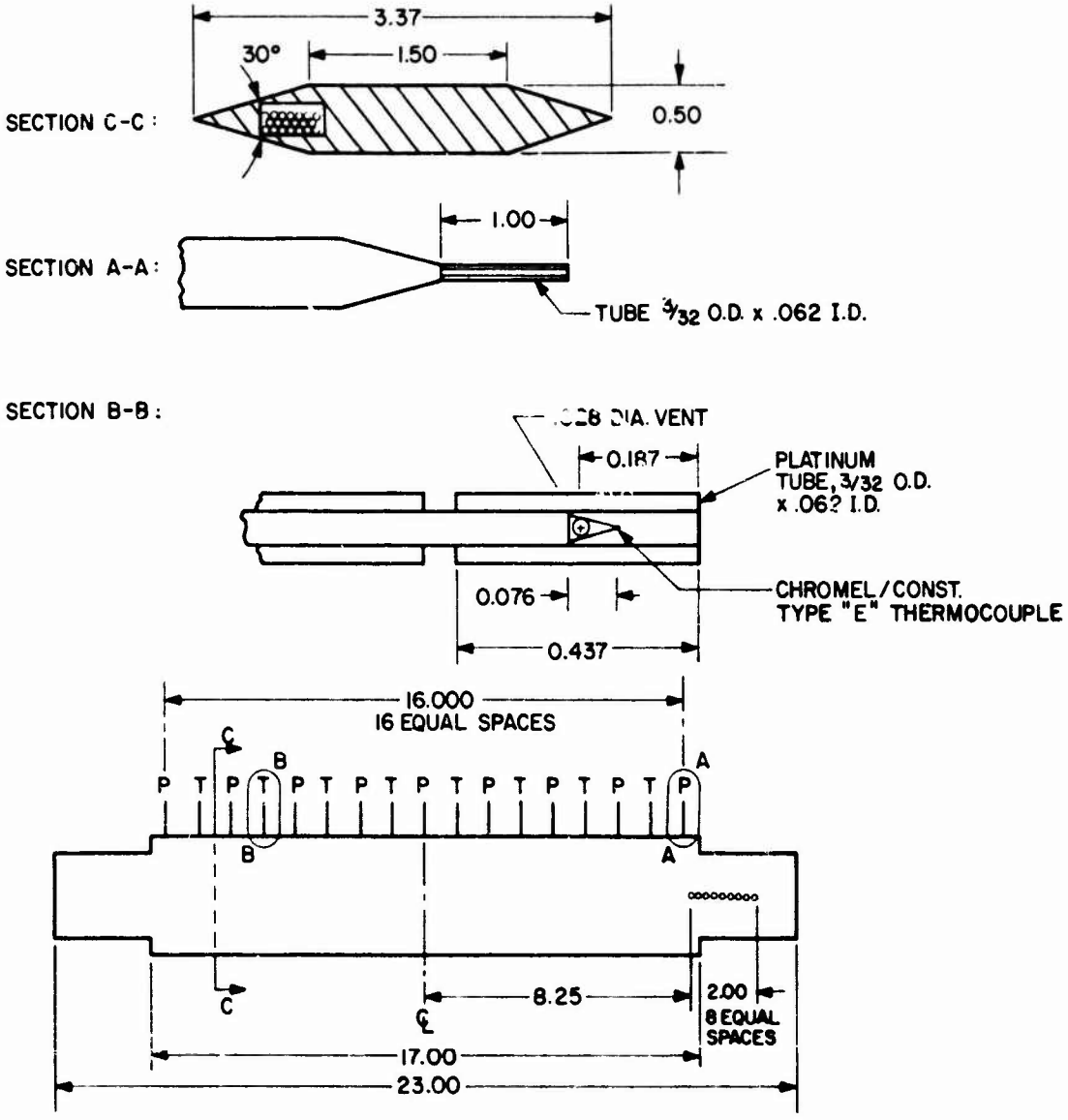

Figure 4. Mach Number and Total Enthalpy Rake

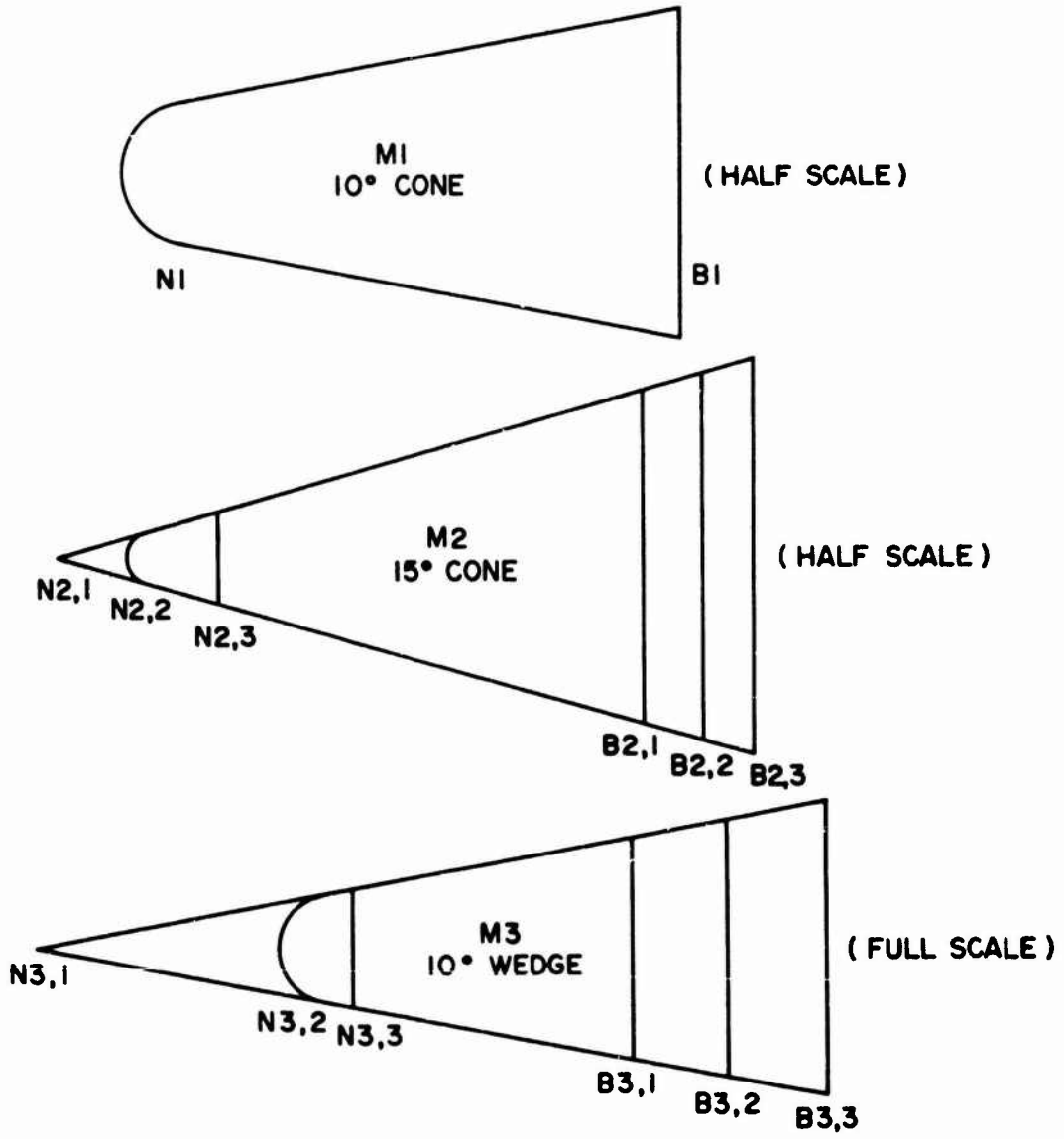

Figure 5. Blockage Model Configurations

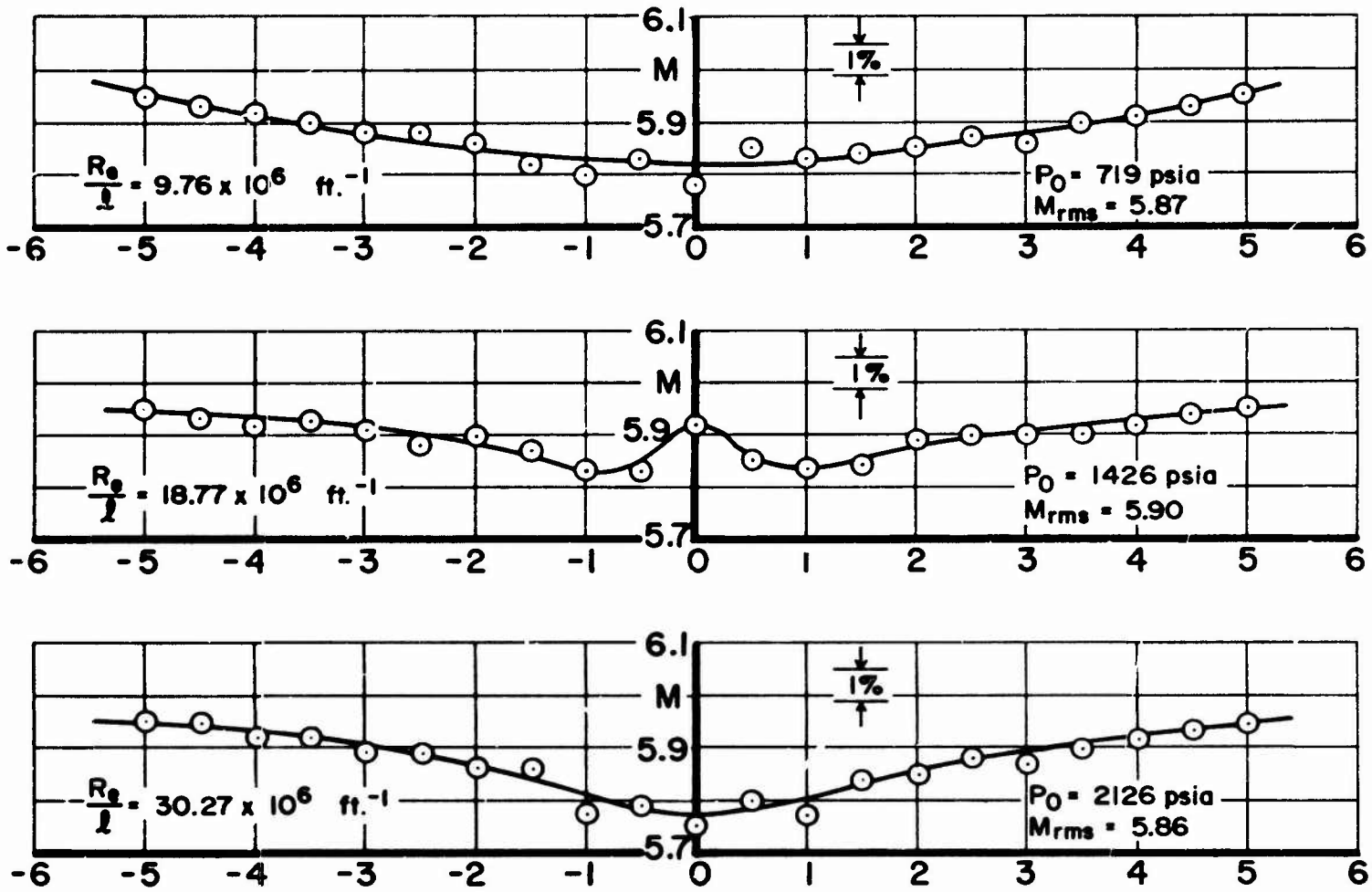

Figure 6. Lateral Mach Number Distribution at X = 2.5 Inches for T_o = 1095°R and Various Unit Reynolds Numbers

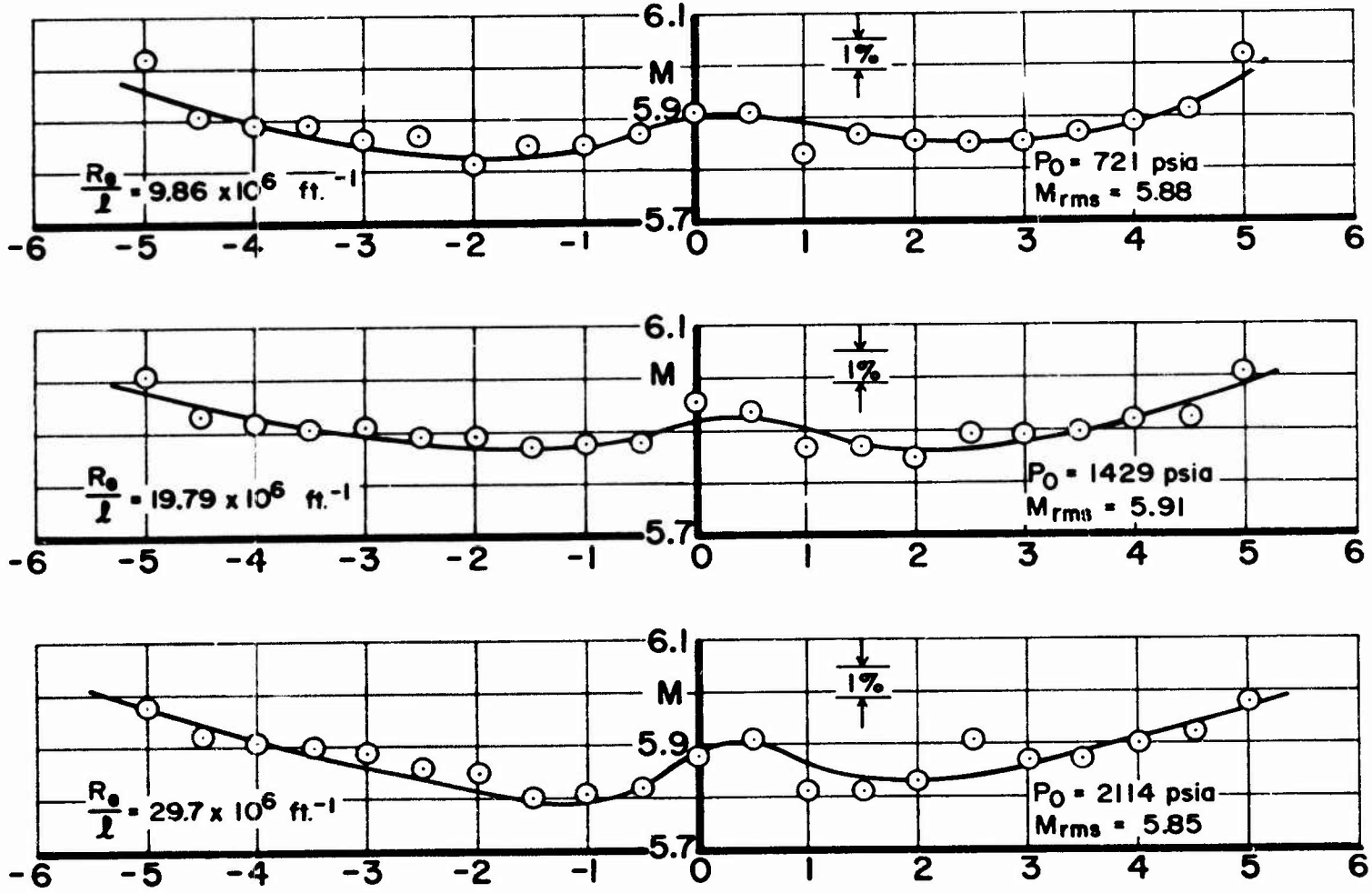

Figure 7. Lateral Mach Number Distribution at X = 5.75 Inches for T_o = 1079°R and Various Unit Reynolds Numbers

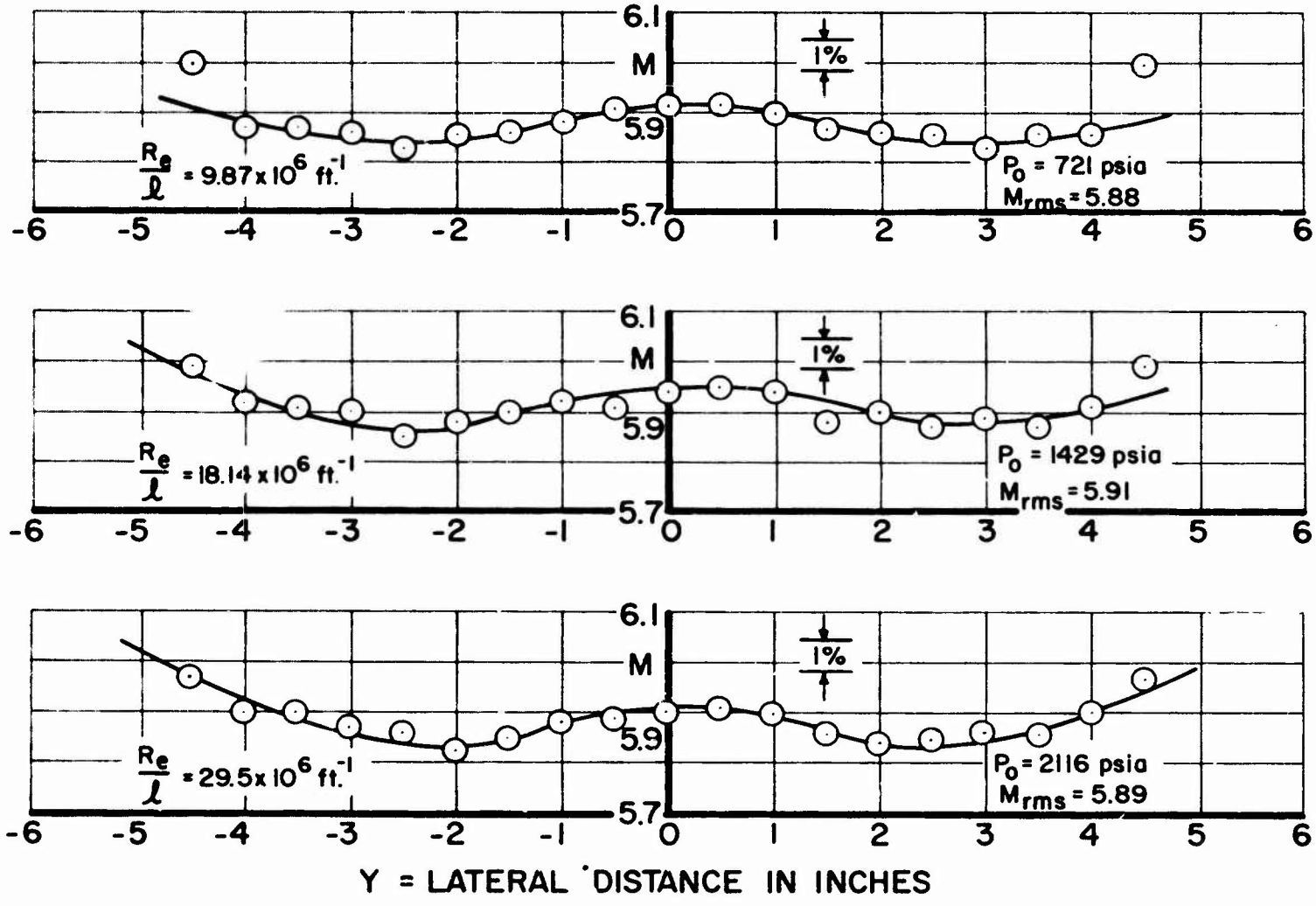

Figure 8. Lateral Mach Number Distribution at X = 9.00 Inches for T_0 = 1071°R and Various Unit Reynolds Numbers

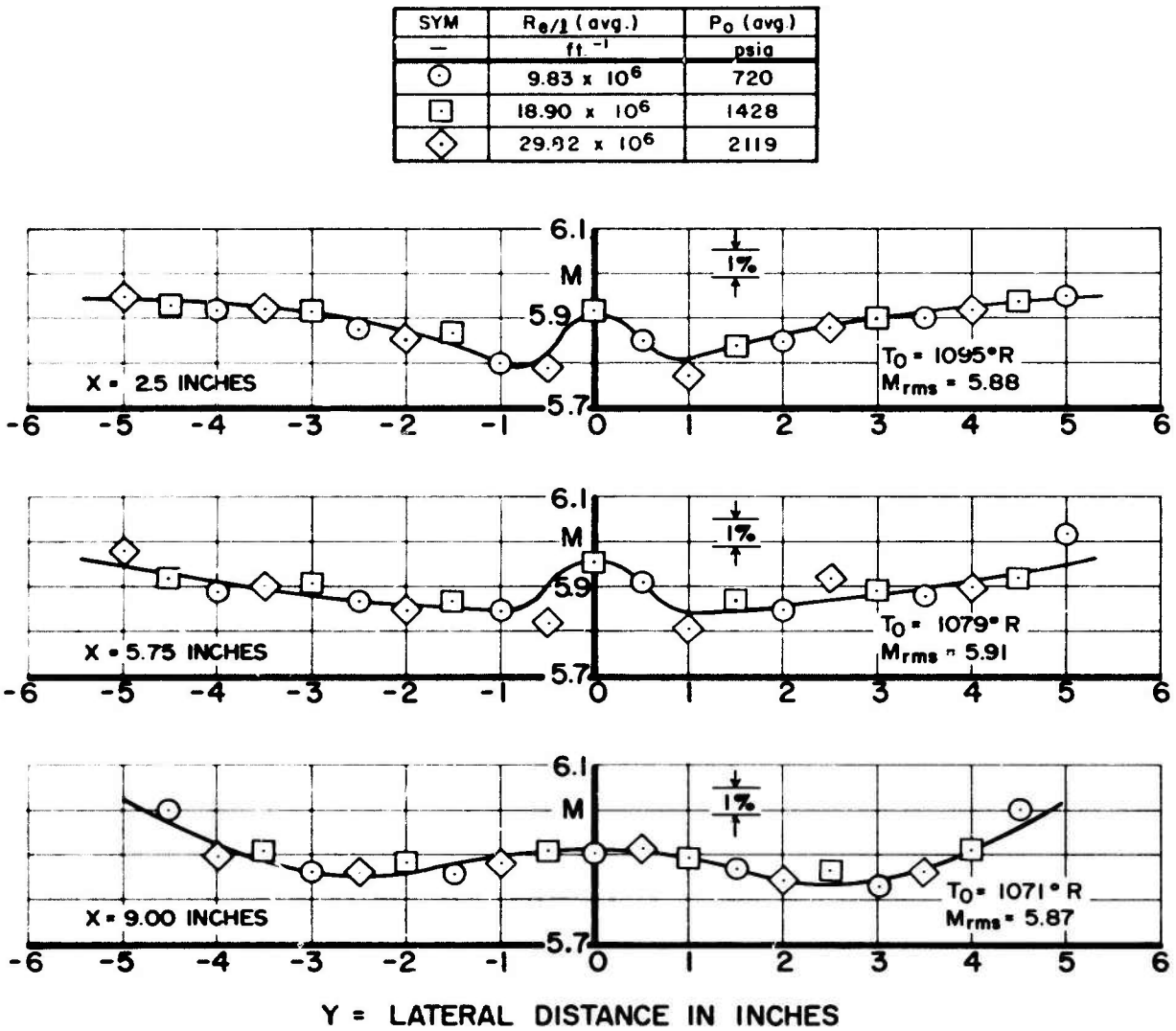

Figure 9. Unit Reynolds Number Effect on the Lateral Mach Number Distribution With Longitudinal Distance as a Parameter

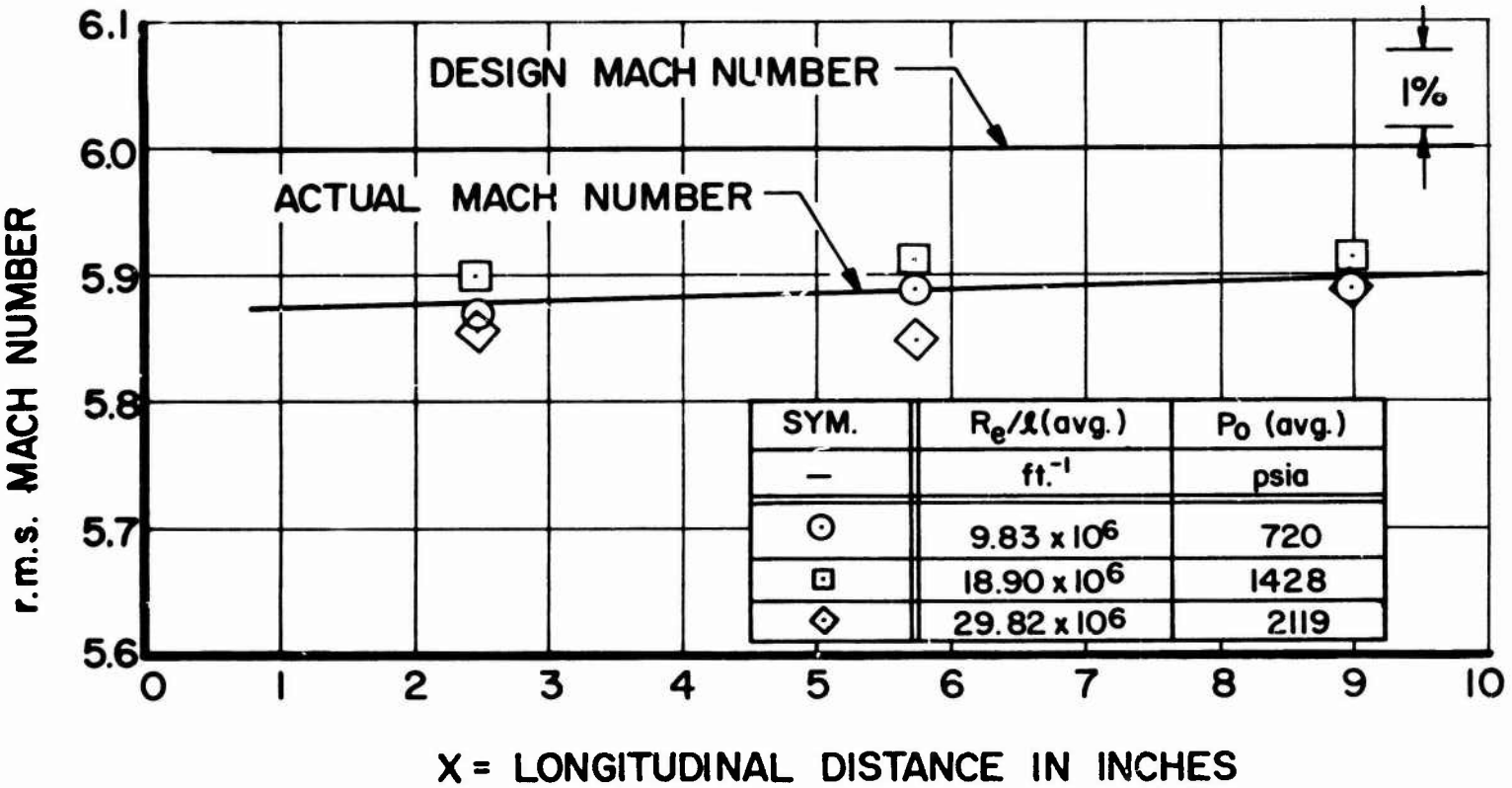

Figure 10. Longitudinal r.m.s. Mach Number Distribution for an Average $T_o = 1082^oR$ and the Average Unit Reynolds Number as a Parameter

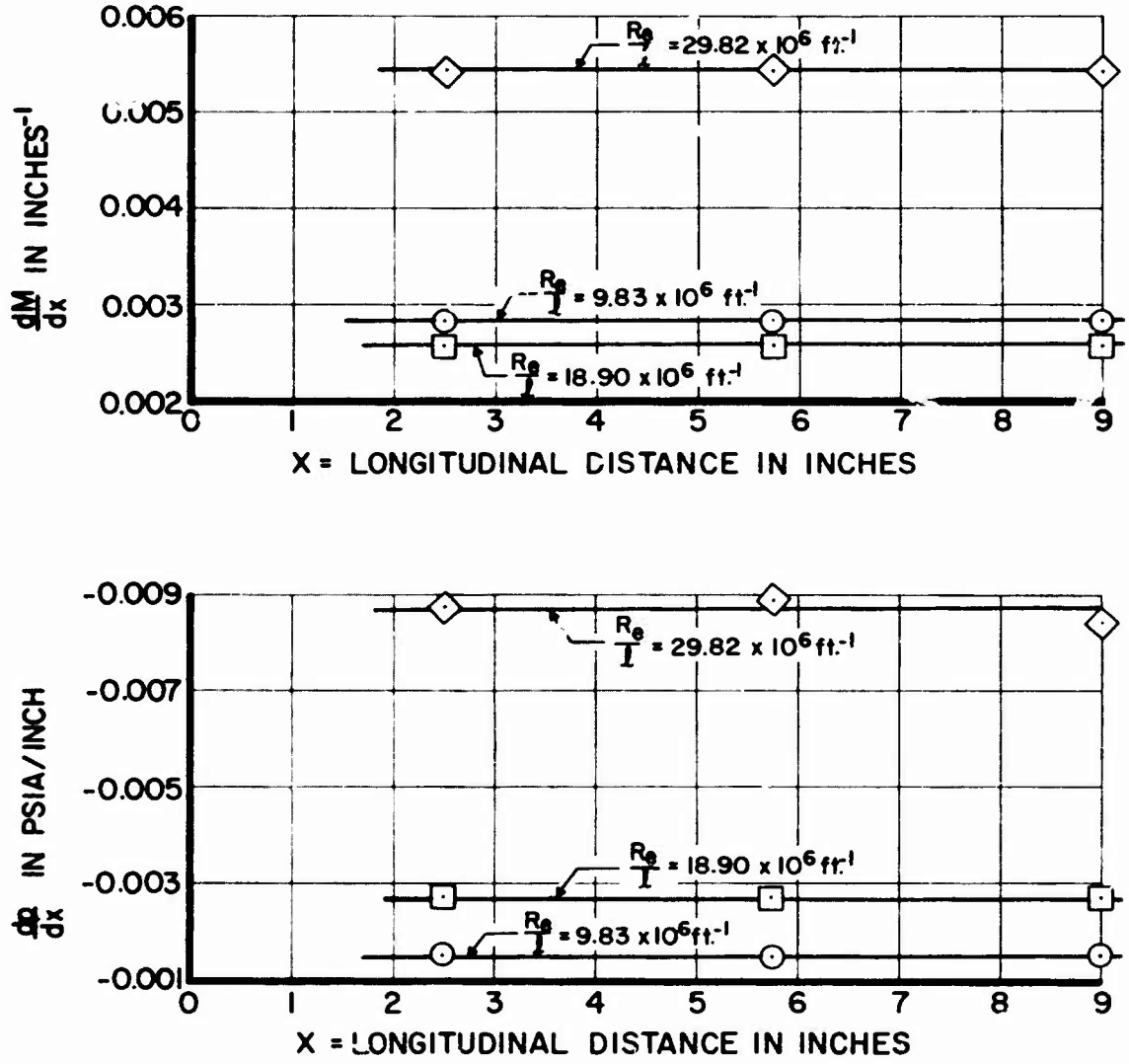

Figure 11. The Longitudinal Mach Number Gradient and the Static Pressure Gradient in the Free Jet With the Average Unit Reynolds Number as a Parameter

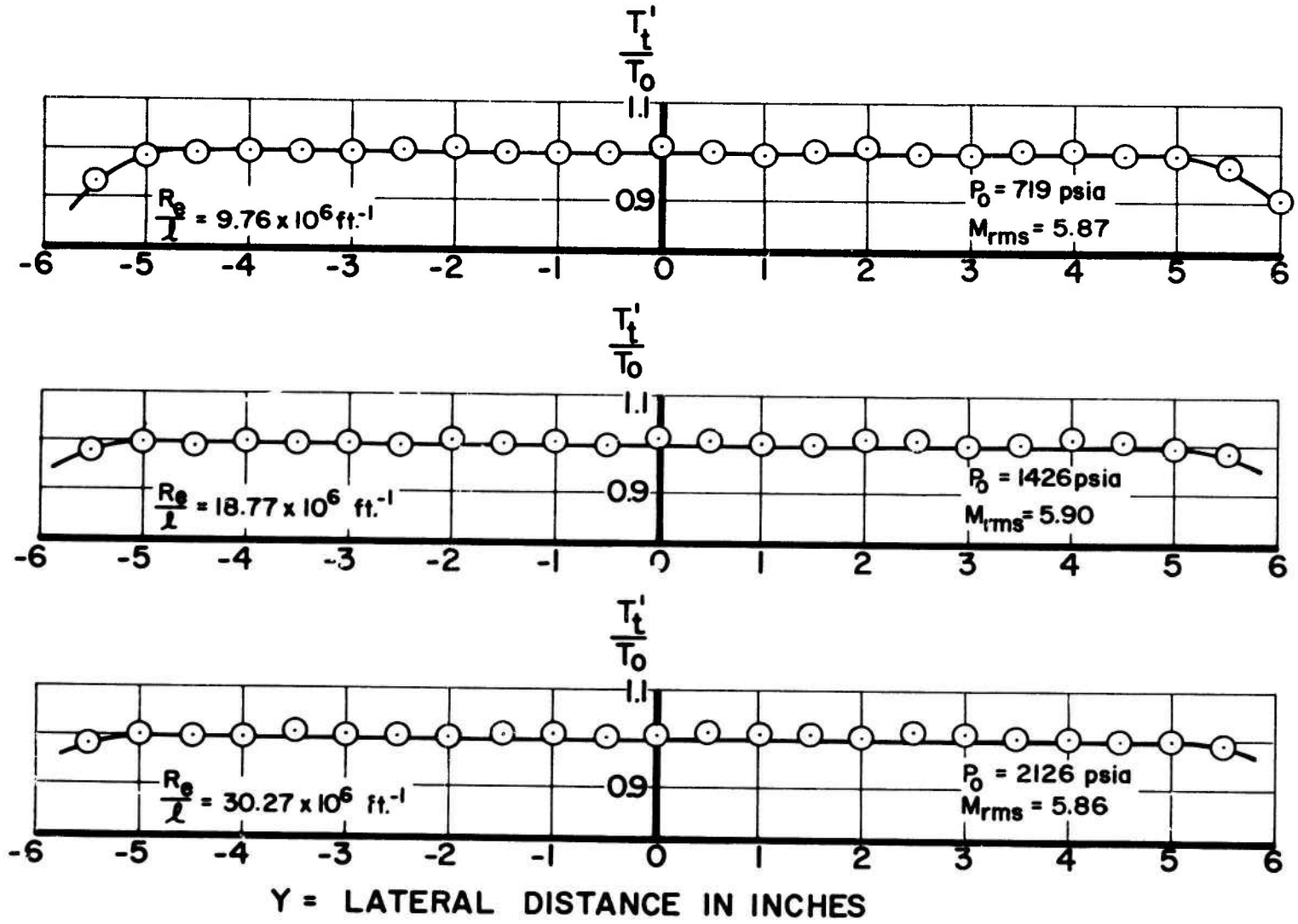

Figure 12. Lateral Total Temperature Distribution at X = 2.5 Inches for T_0 = 1095°R and Various Unit Reynolds Numbers

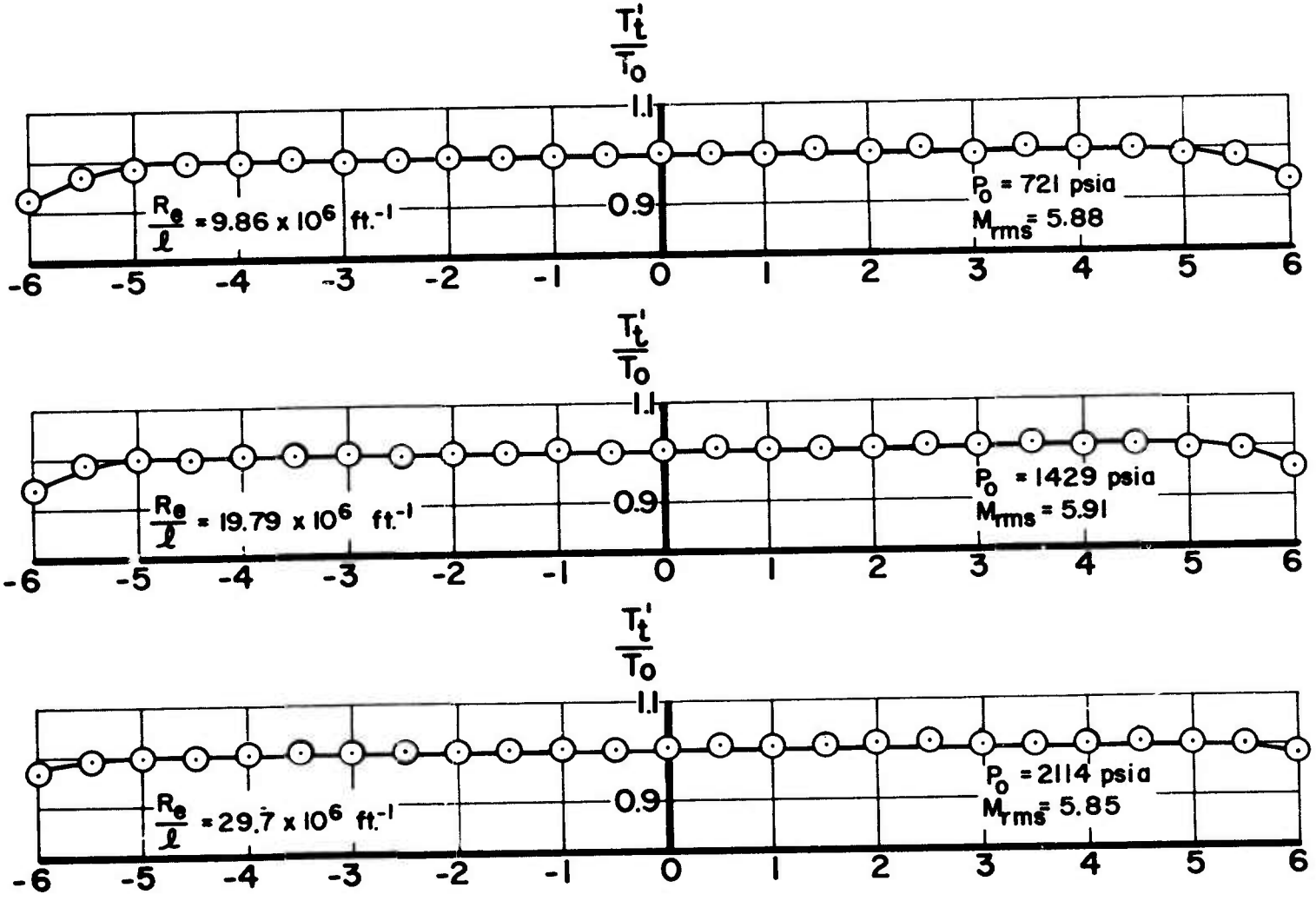

Figure 13. Lateral Total Temperature Distribution at X = 5.75 Inches for T_o = 1079°R and Various Unit Reynolds Numbers

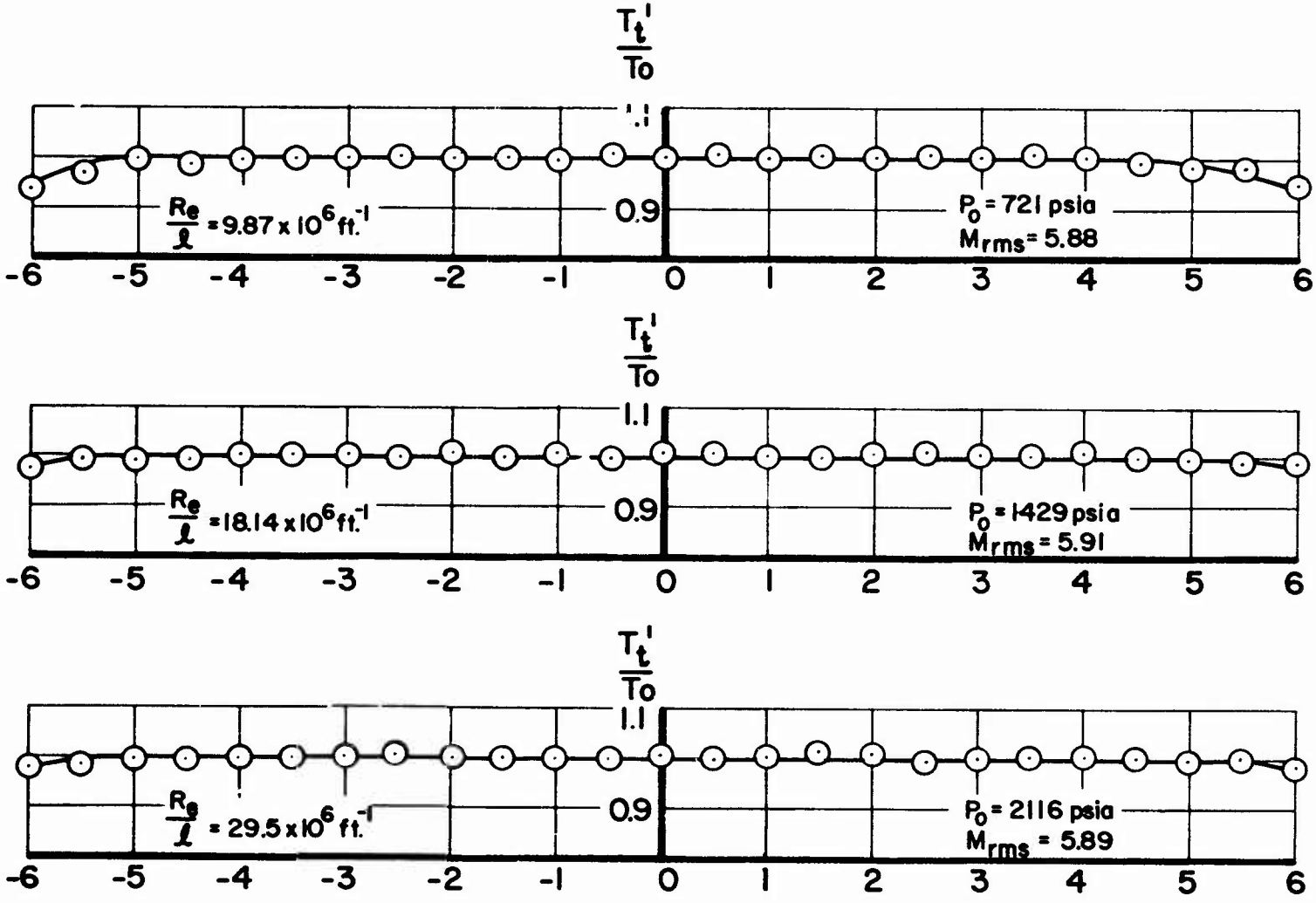

Figure 14. Lateral Total Temperature Distribution at X = 9.00 Inches for T_o = 1071°R and Various Unit Reynolds Numbers

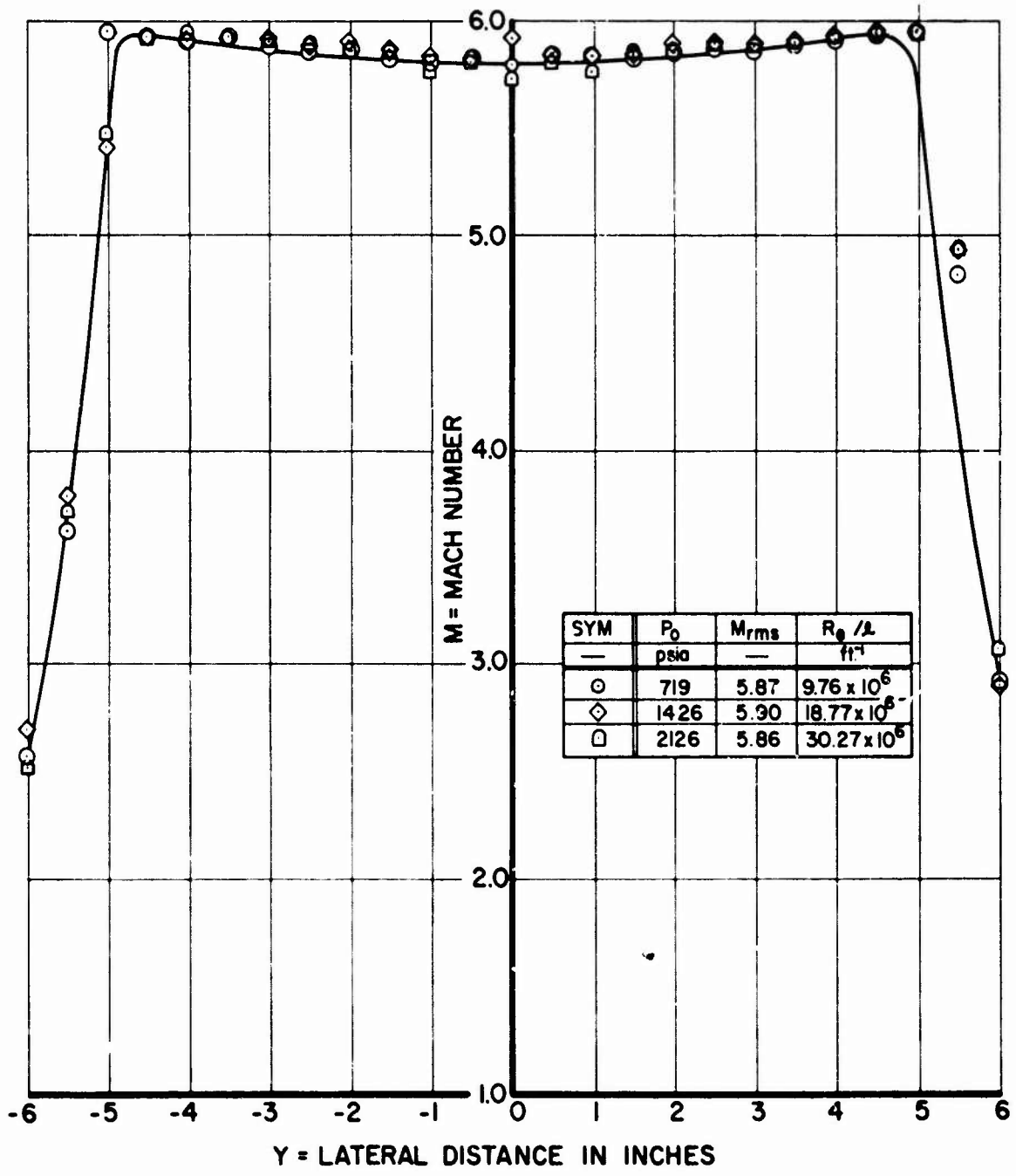

Figure 15. Lateral Mach Number Distribution at X = 2.5 Inches for $T_0 = 1095^0R$ With the Unit Reynolds Number as a Parameter

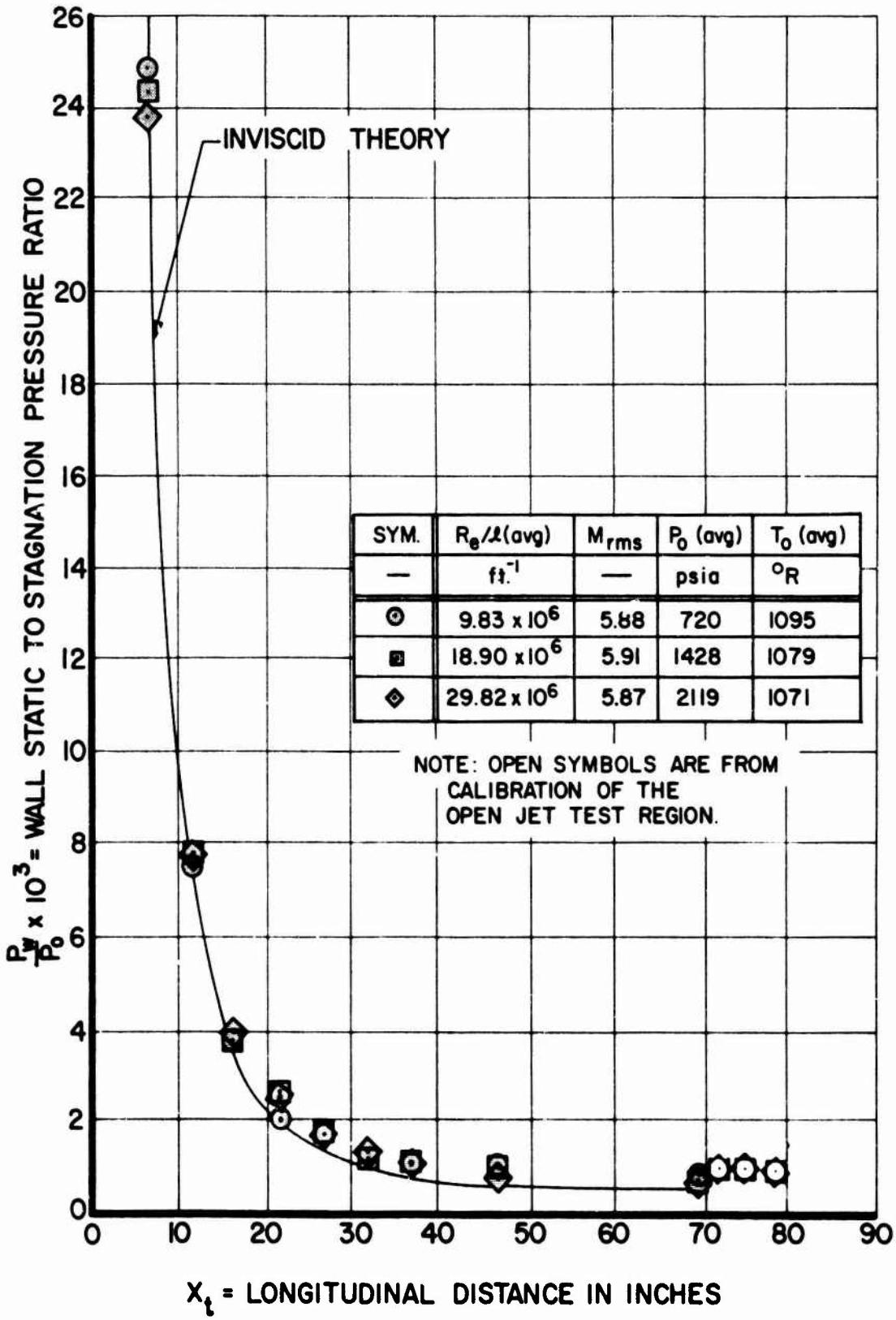

Figure 16. The Wall Static Pressure Versus the Longitudinal Distance From The Tunnel Throat With the Unit Reynolds Number as a Parameter

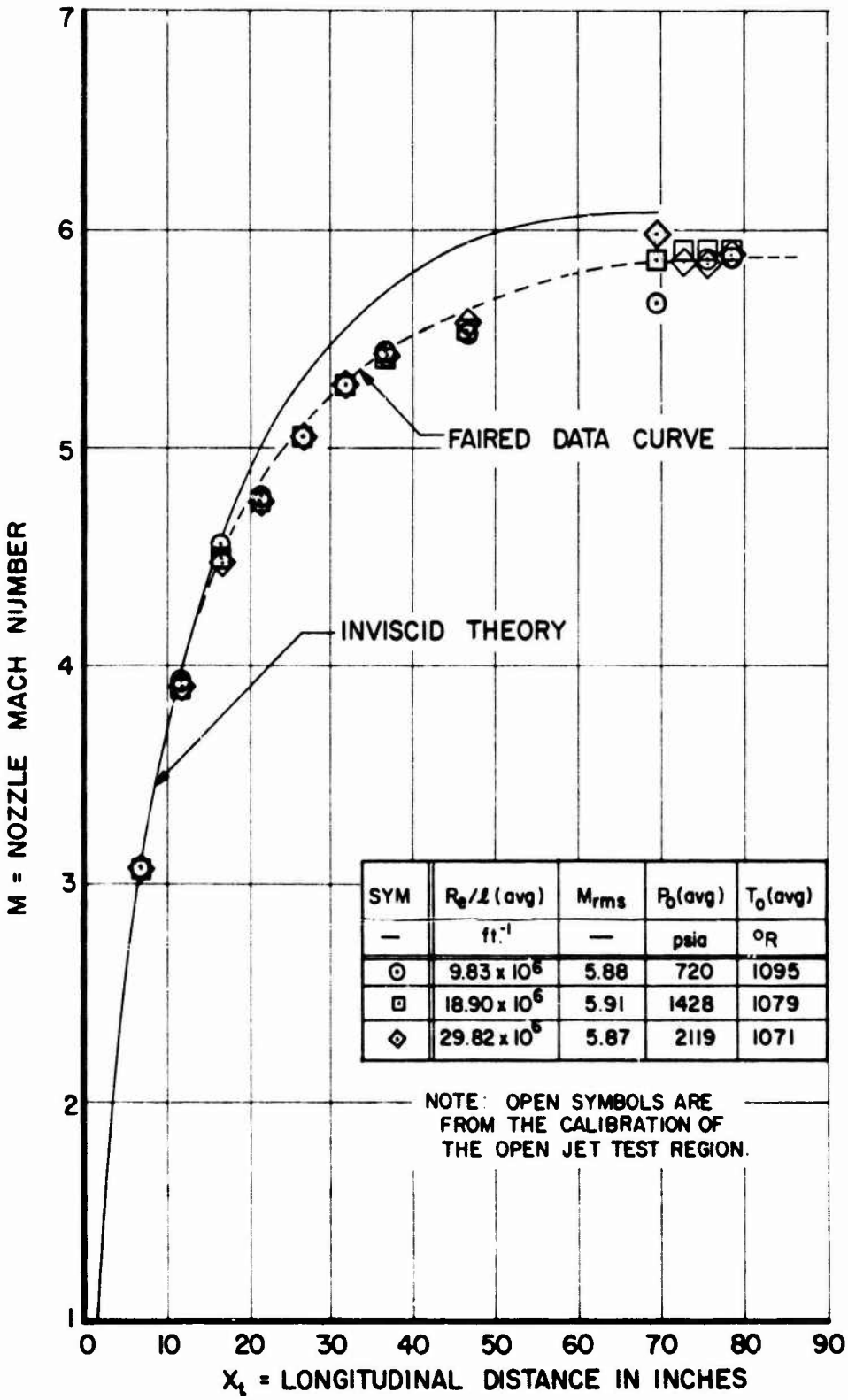

Figure 17. Nozzle Mach Number Versus the Longitudinal Distance From the Tunnel Throat With the Unit Reynolds Number as a Parameter

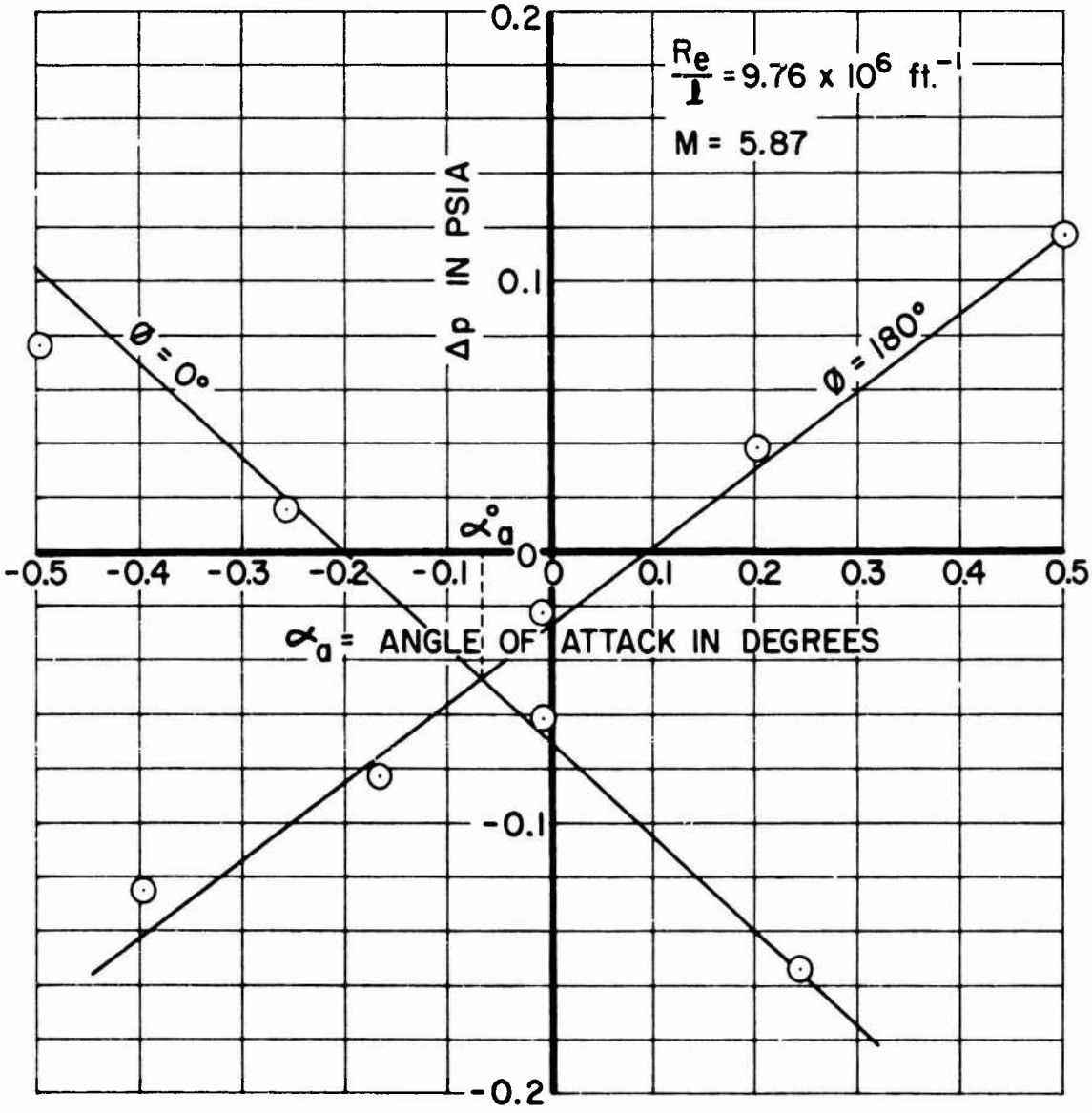

Figure 18. Surface Pressure Difference Versus Angle of Attack For P_0 = 719 psia and T_0 = 1095°R at X = 2.5 Inches and Y = +3.67 Inches

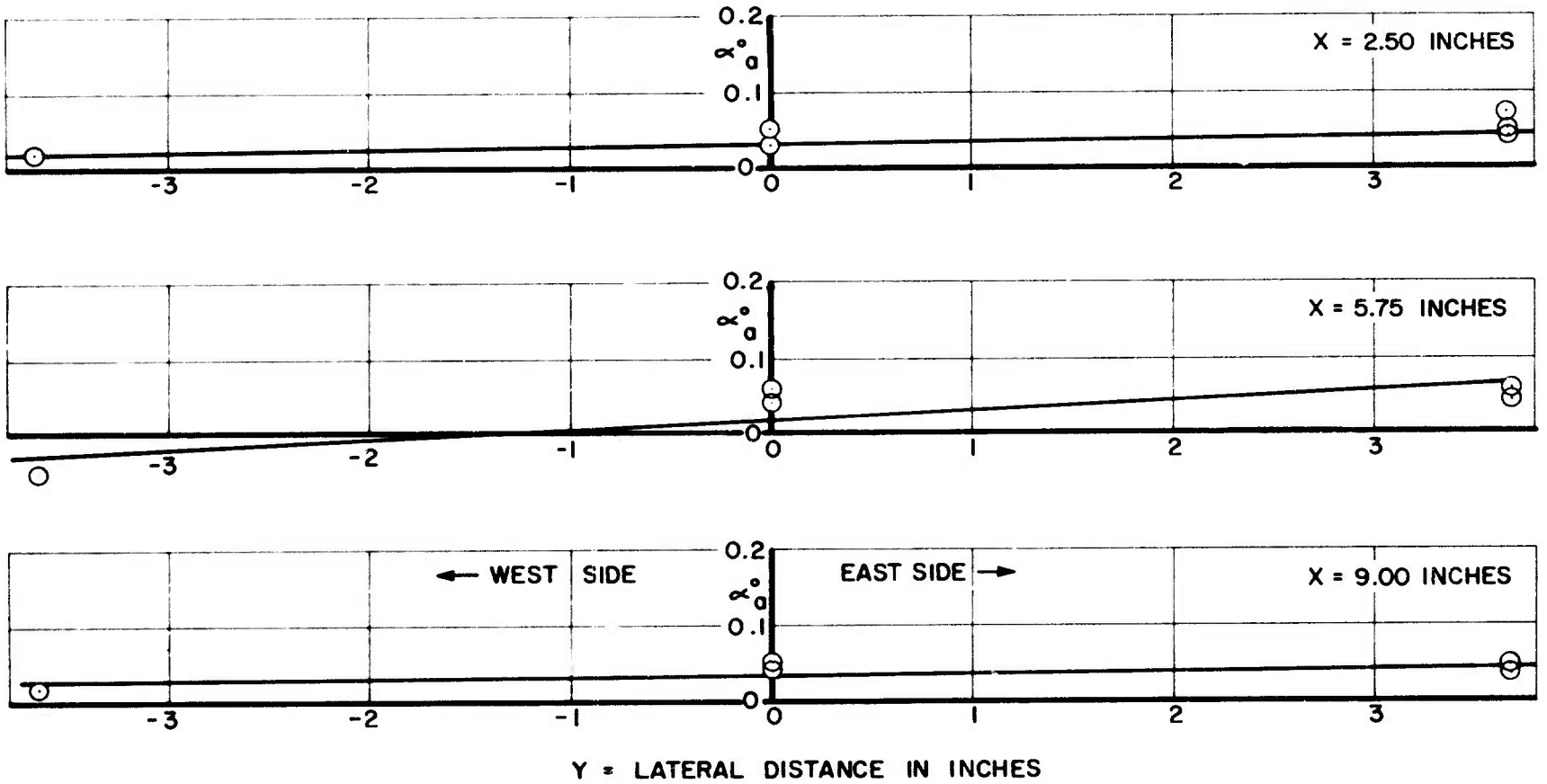

Figure 19. Flow Angularity Versus Lateral Distance for P_o = 719 psia, T = 1095°R, M = 5.87, and $R_{e/\ell}$ = 9.76 x 10^6 ft.$^{-1}$

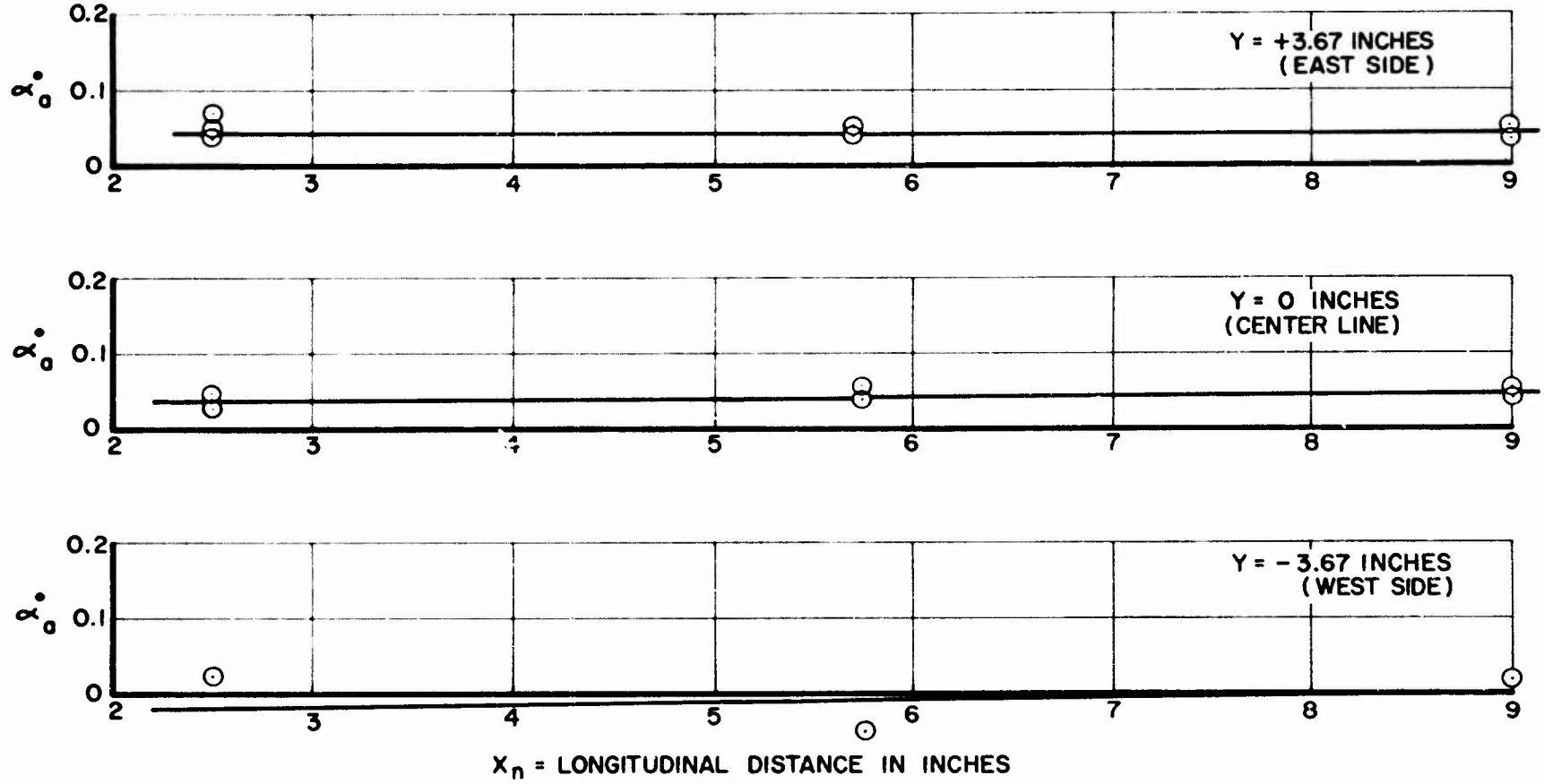

Figure 20. Flow Angularity Versus Longitudinal Distance From Nozzle Outlet for P_o = 719 psia, T_o = 1095°R, M = 5.87 and $R_{e/\ell}$ = 9.76 x 10^6 ft.$^{-1}$

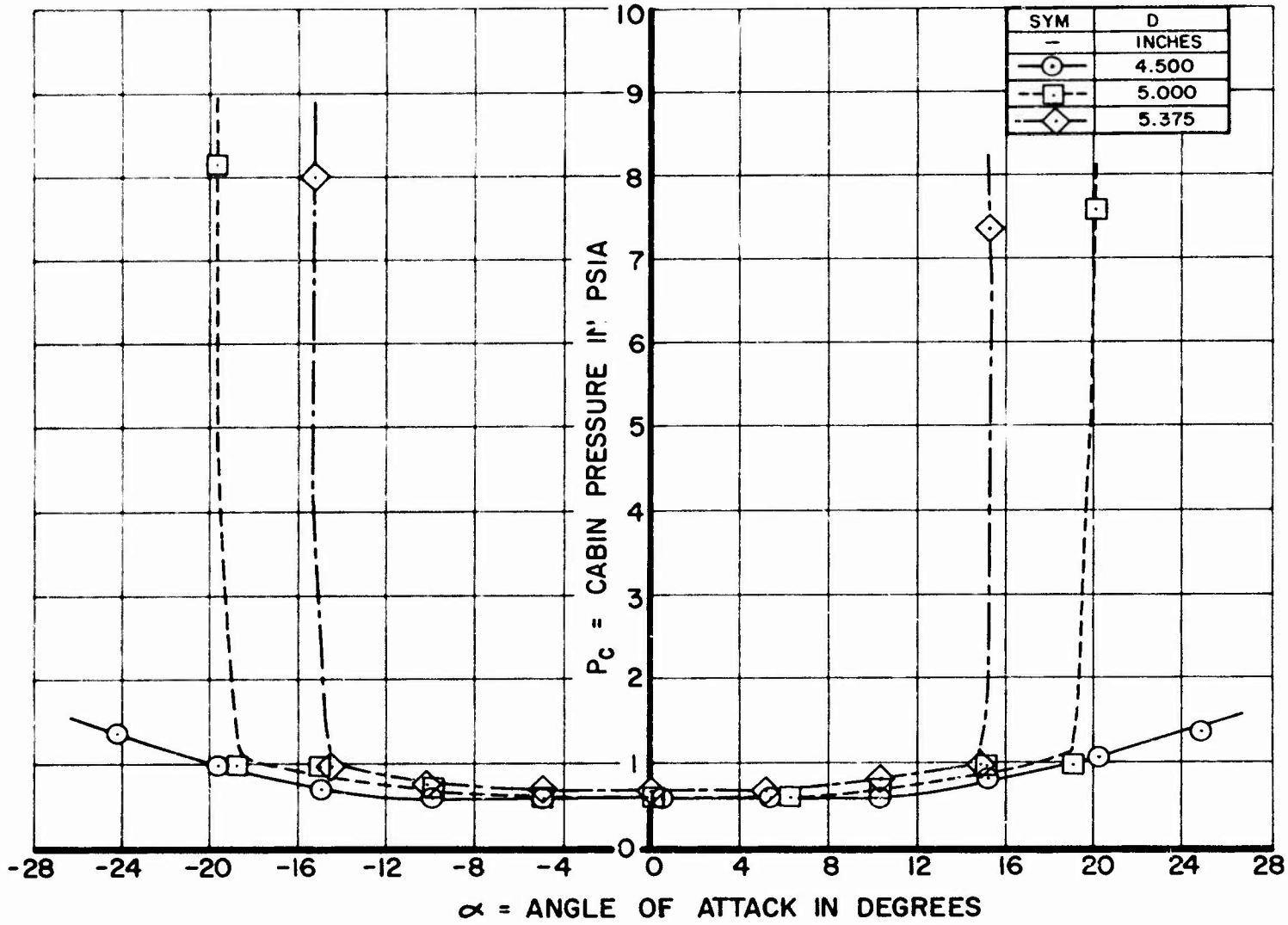

Figure 21. Cabin Pressure Versus Angle of Attack With Model Base Diameter as a Parameter for a 15^{o} Cone With a Sharp Nose (N2,1) at M = 5.88 and $R_{e/\ell} = 9.76 \times 10^{6}$ ft.$^{-1}$

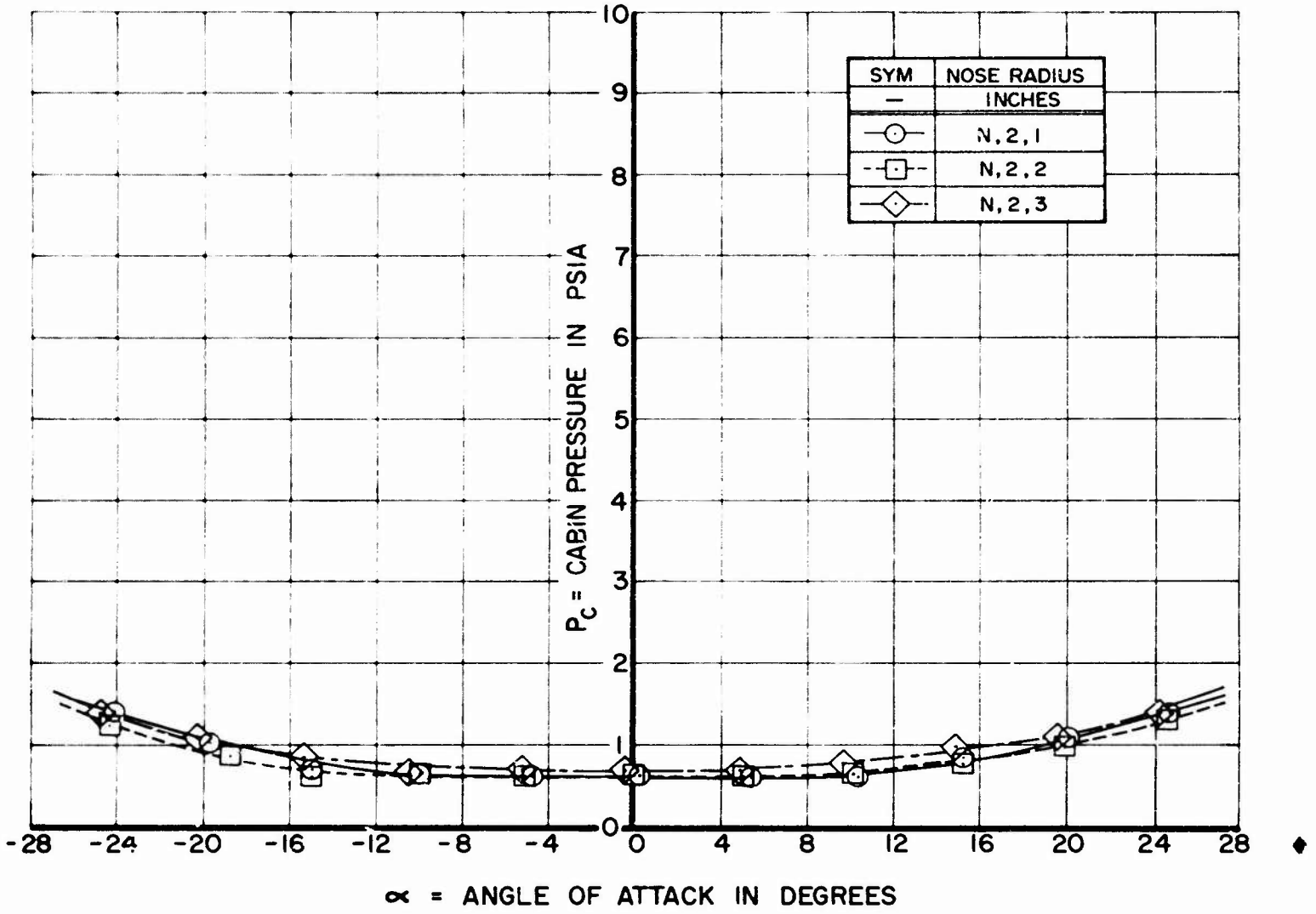

Figure 22. Cabin Pressure Versus Angle of Attack With Model Nose Radius as a Parameter for a 15° Cone With a Base Diameter of 4.5 Inches at M = 5.88 and $R_{e/\ell}$ = 9.76 x 10^6 ft.$^{-1}$

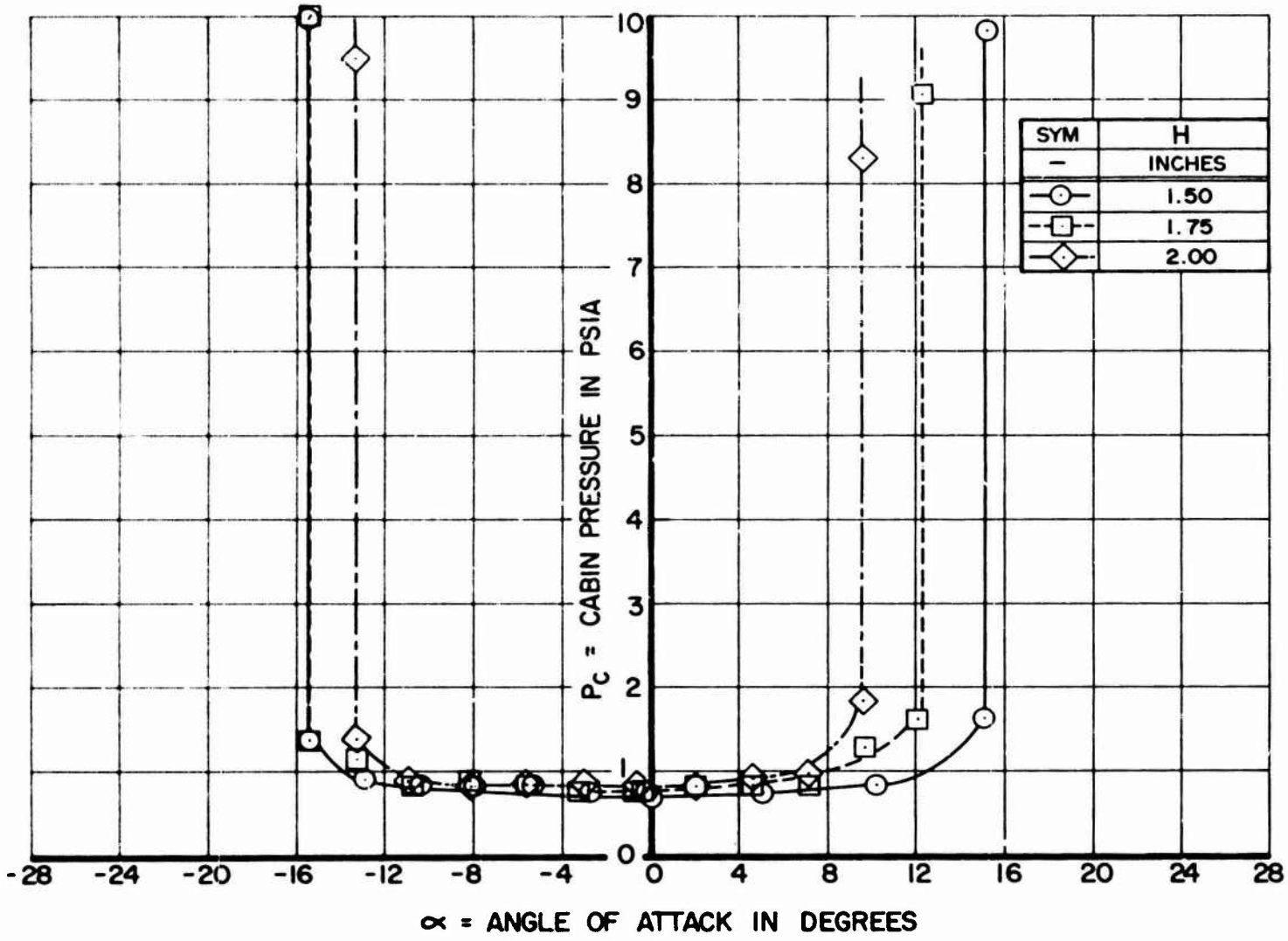

Figure 23. Cabin Pressure Versus Angle of Attack With Model Base Height as a Parameter for a 10° Wedge With a Sharp Nose (N3,1) at M = 5.88 and $R_{e/\ell} = 9.76 \times 10^6$ ft.$^{-1}$

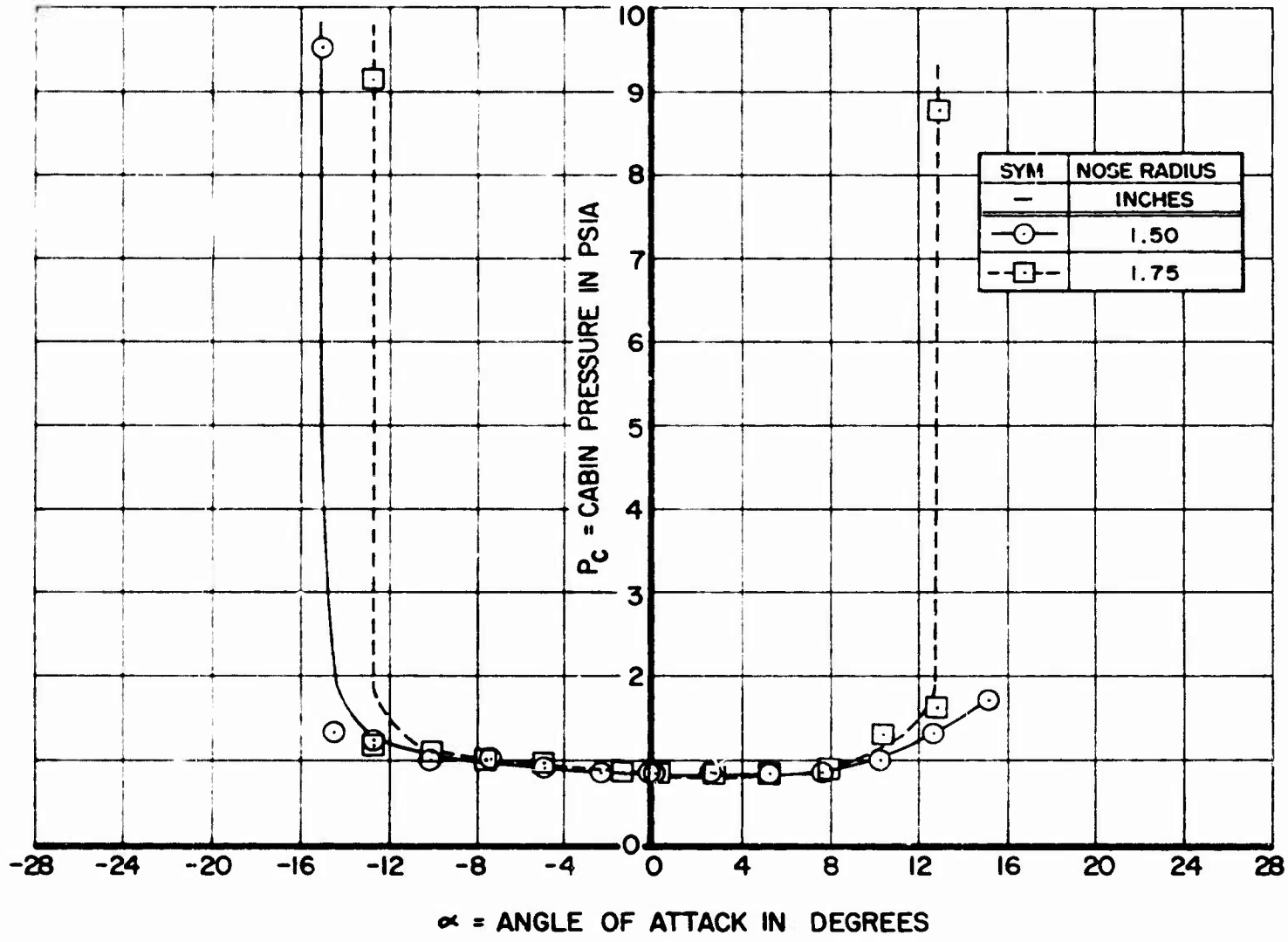

Figure 24. Cabin Pressure Versus Angle of Attack With Model Base Height as a Parameter for a 10^{0} Wedge With a Round Nose (N,3,2) at M = 5.88 and $R_{e/\ell} = 9.76 \times 10^{6}$ ft.$^{-1}$

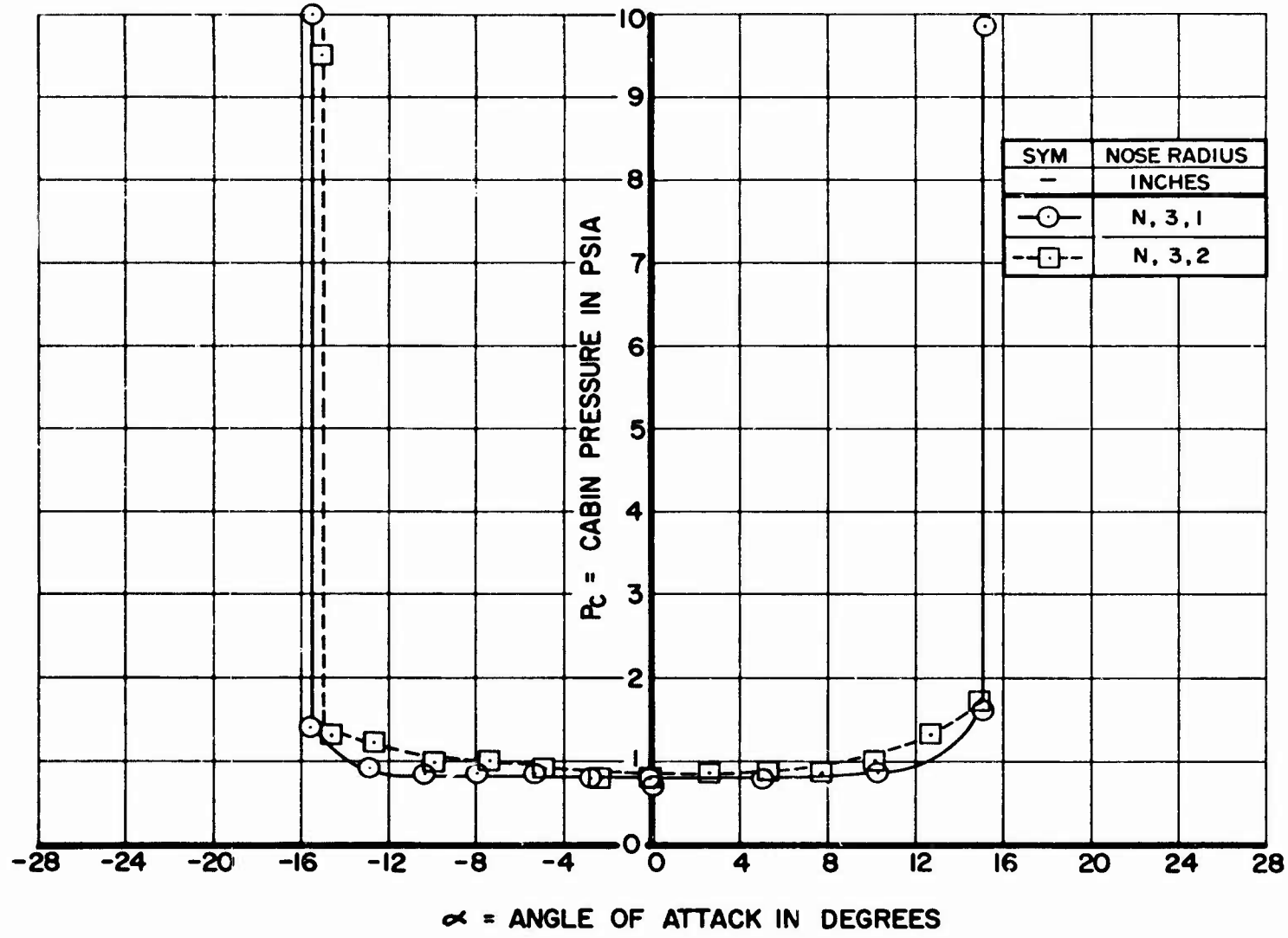

Figure 25. Cabin Pressure Versus Angle of Attack With Nose Radius as a Parameter for a 10^0 Wedge With a 1.5 Inch Base Height at M = 5.88 and $R_{e/\ell} = 9.76 \times 10^6$ ft.$^{-1}$

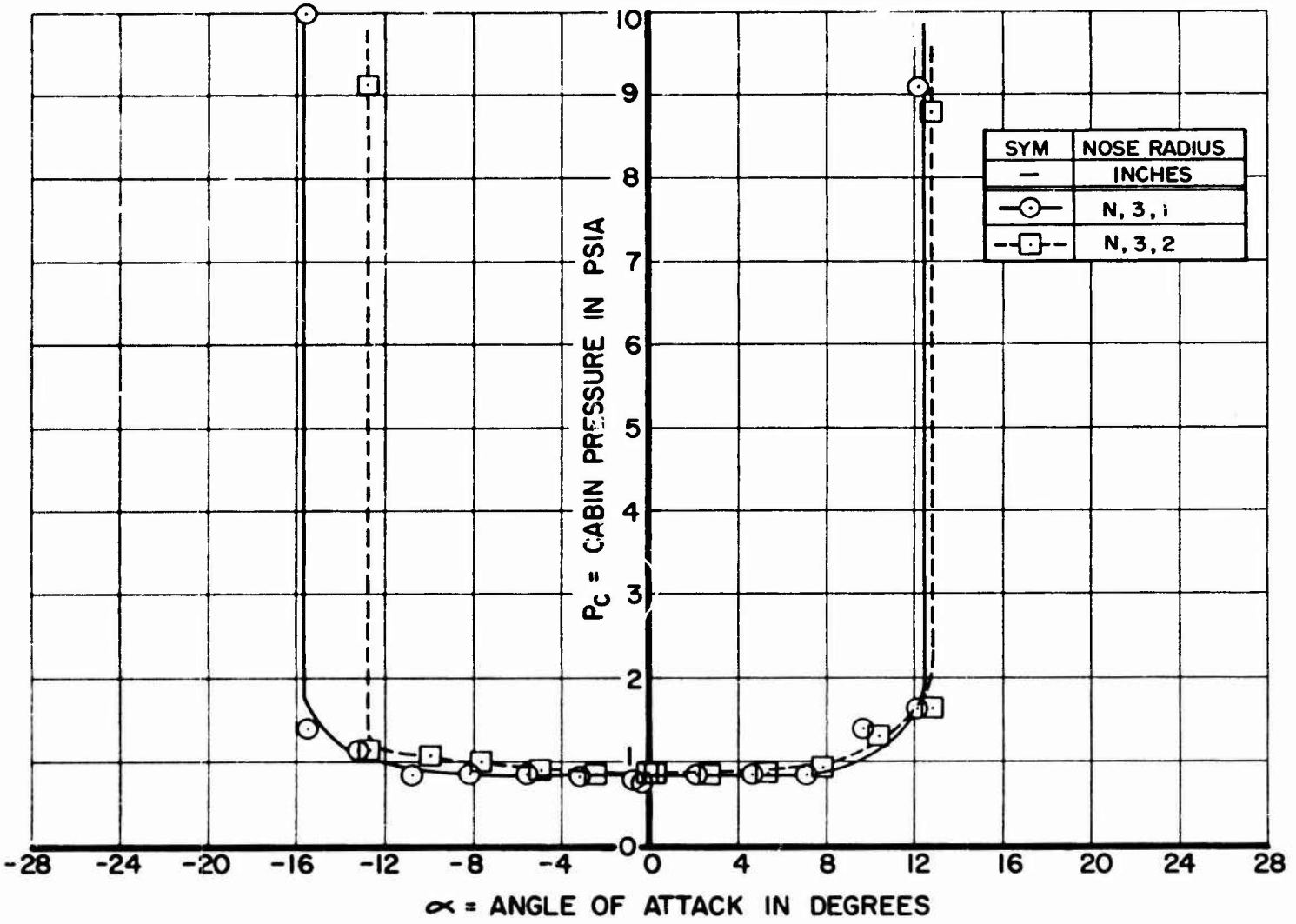

Figure 26. Cabin Pressure Versus Angle of Attack With Nose Radius as a Parameter for a 10^0 Wedge With a 1.75 Inch Base Height at M = 5.88 and $R_{e/\ell} = 9.76 \times 10^6$ ft.$^{-1}$

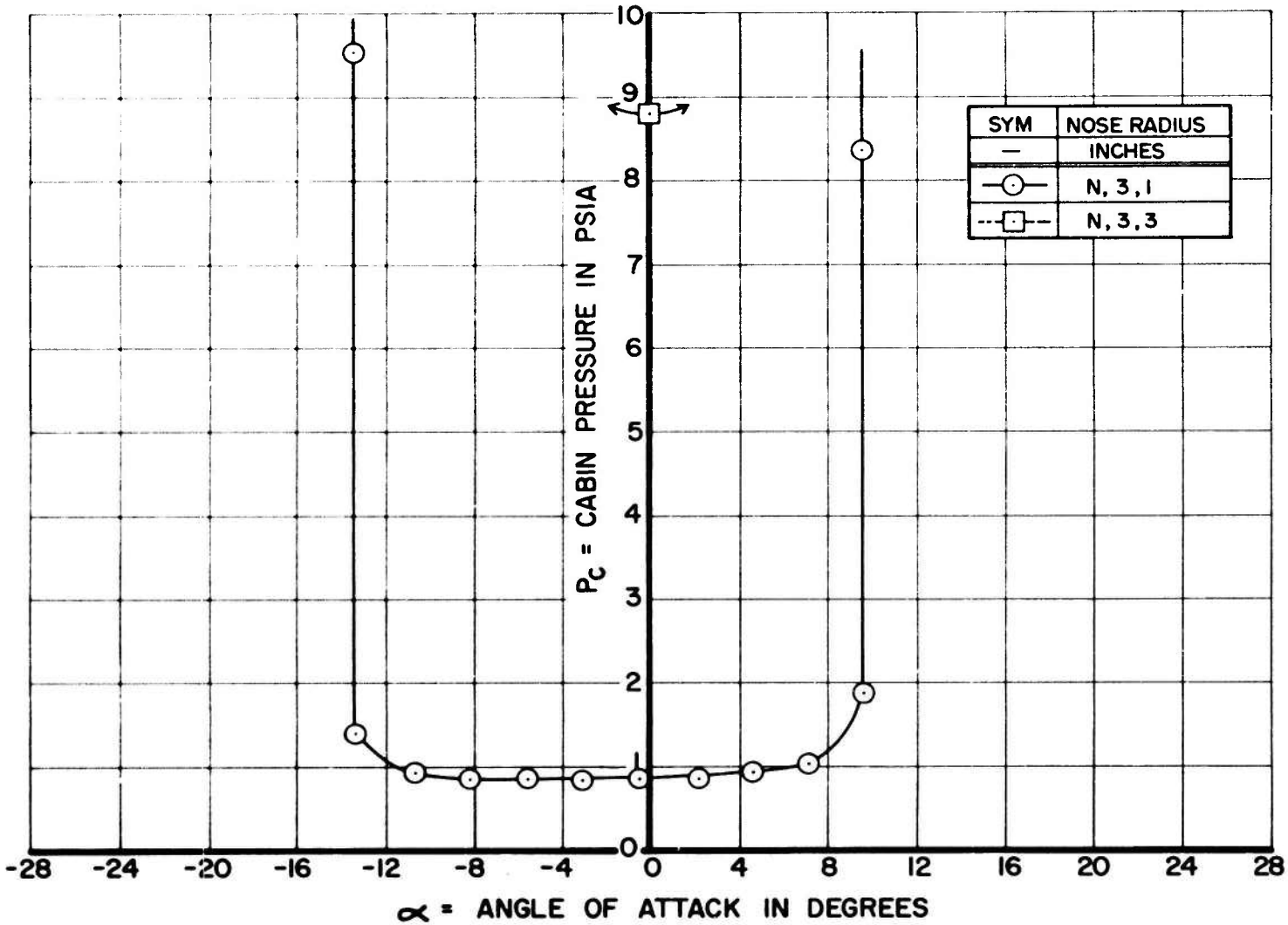

Figure 27. Cabin Pressure Versus Angle of Attack With Nose Radius as a Parameter for a 10^{o} Wedge With a 2.00 Inch Base Height at M = 5.88 and $R_{e/\ell} = 9.76 \times 10^{6}$ ft.$^{-1}$

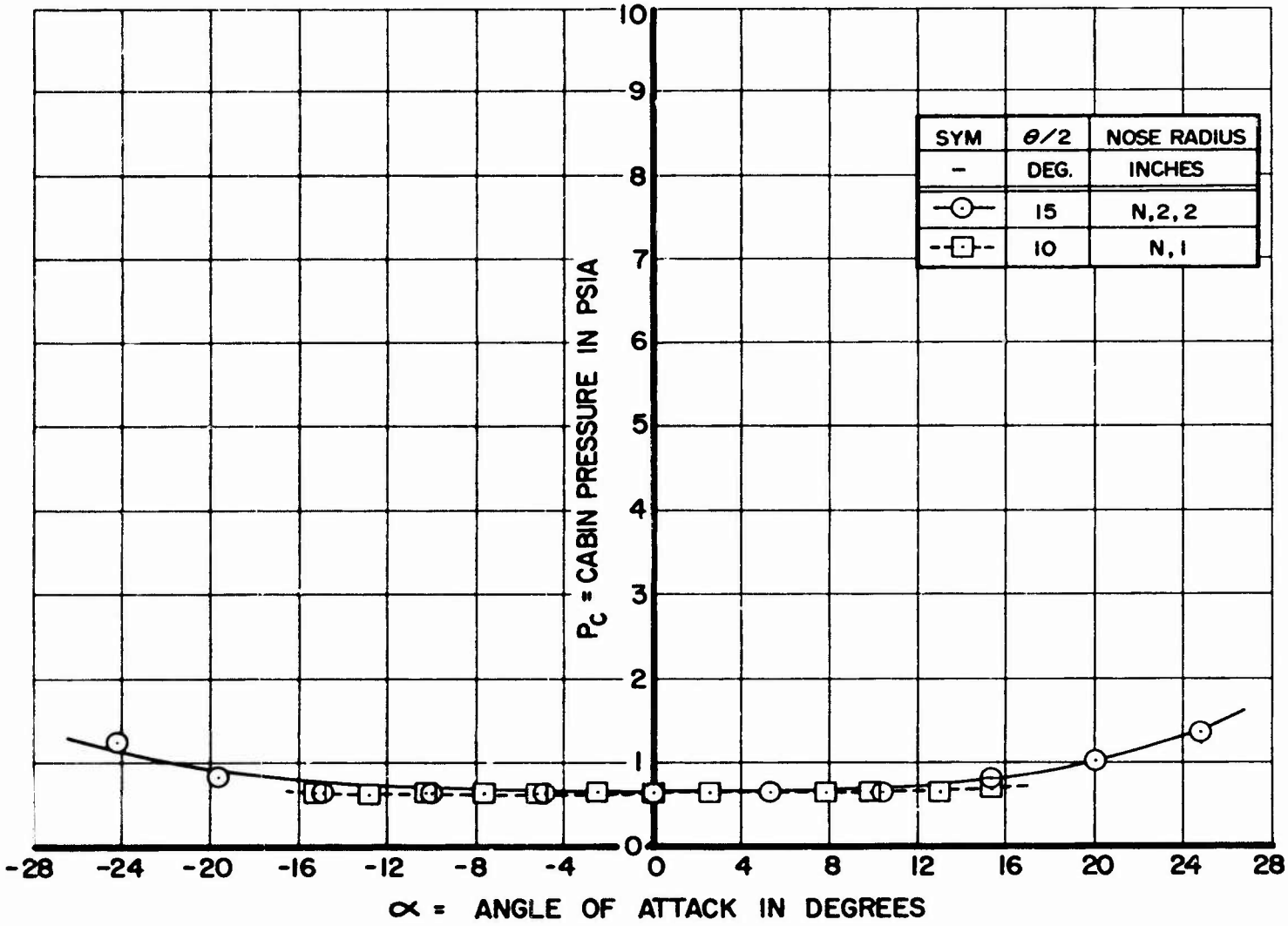

Figure 28. Cabin Pressure Versus Angle of Attack With Half Angle and Nose Radius as a Parameter for Cones With a 4.5 Inch Diameter at M = 5.88 and $R_{e/\ell} = 9.76 \times 10^6$ ft.$^{-1}$

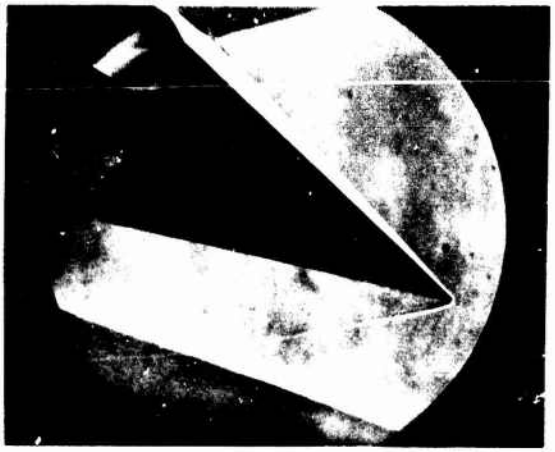

D = 4.5 IN. ; α = -25°

D = 4.5 IN. ; α = +25°

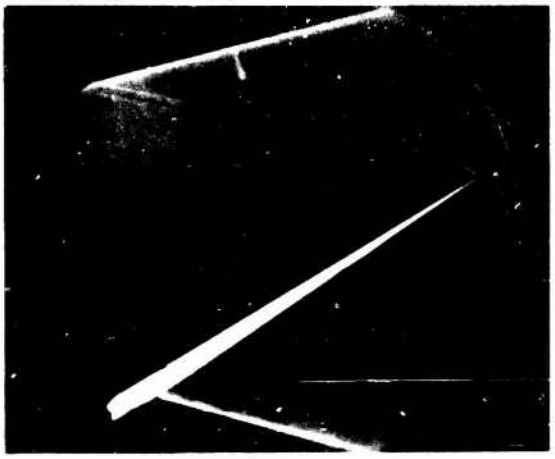

D = 5 IN. ; α = +15°

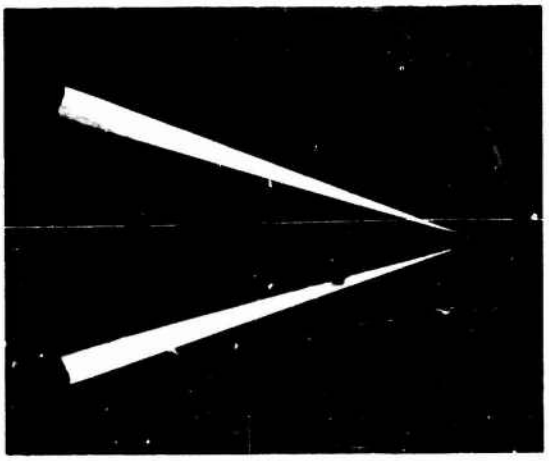

D = 5.375 IN. ; α = 0°

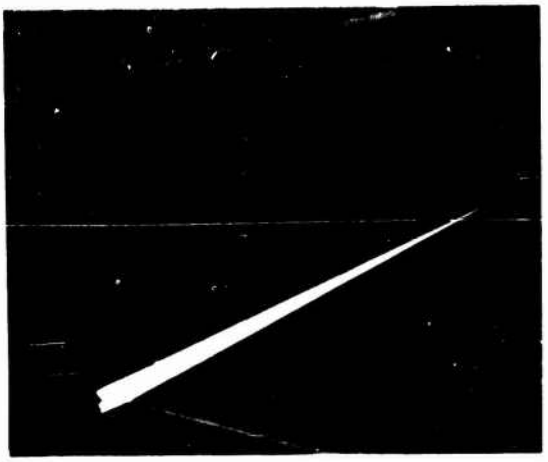

D = 5.375 IN. ; α = +10°

Figure 29. Schlieren of 15° Cone With Sharp Nose (N2,1) at M = 5.88 and $\frac{Re}{\ell}$ = 9.76 x 10^6 per foot

REFERENCES

1. Fiore, A. W.; Moore, D.; Murray, D.; and West, J.; "Design and Calibration of the M=3 High Reynolds Number Facility," ARL 75-0012.

2. Baron, J. R.; "Analytic Design of a Family of Supersonic Nozzles by The Fredricks Method". WADC Technical Report 54-279. AD 55-902, Naval Supersonic Laboratory MIT, June 1954.

3. Fiore, A. W.; "Turbulent Boundary Layer Measurements At Hypersonic Mach Numbers". ARL 70-0166 dated August 1970.

4. Ames Research Staff, "Equations, Tables, and Charts for Compressible Flow," NACA Report 1135, 1957.

5. Fiore, A. W.; "The Use of Conical Nozzles In A Hypersonic Wind Tunnel". O.A.R. Vol III, No: 8, October 1964.

6. Dayman, Bane Jr. and Fiore, A. W.; "Part 2 - Aerodynamic Testing and Simulation: Saving Lives, Time and Money". Astronautics & Aeronautics. June 1974.

7. Schueler, C. J.; "An Investigation of Model Blockage for Wind Tunnels at Mach Numbers 1.5 to 19.5". AEDC TN 59-165, 1960.

LIST OF SYMBOLS

P_o = Tunnel stagnation pressure in psia.

T_o = Tunnel stagnation temperature in Degrees Rankine.

M = Mach Number.

R_e = Reynolds Number based on free stream condition.

ℓ = Reference length in feet.

X = Distance from the nozzle outlet in inches.

Y = Lateral distance from the tunnel centerline in inches.

$\frac{dM}{dx}$ = Mach Number longitudinal gradient in per inch.

$\frac{dM}{dy}$ = Mach Number lateral gradient in per inch.

$\frac{dp}{dx}$ = Longitudinal static pressure gradient in psia/inch.

$\frac{dp}{dy}$ = Lateral static pressure gradient in psia/inch.

T_t = Total temperature in the free jet in Degrees Rankine.

P_w = Nozzle wall static pressure in psia.

α = Cone angle of attack in degrees.

Δp : $p_\ell - p_u$ = Cone surface pressure difference in psia.

ϕ = Cone (rolled) position in degrees.

α_a = Flow angularity in degrees.

p = Static pressure in psia.

r = Local nozzle radius in inches.

γ = Ratio of specific heats for air taken as 1.40.

Sub-scripts

r.m.s. = root-mean-square valves.

u = upper surface

ℓ = lower surface

*U.S.Government Printing Office: 1975 — 657-023/664